N-37890

AN EXPERIMENTAL AND ANALYTICAL INVESTIGATION OF THE FLUTTER AND DIVERGENCE OF LARGE MASSES AT THE ENDS OF SHORT STRUTS

A Thesis

Presented to

the Faculty of the Department of Engineering

University of Virginia

In Partial Fulfillment

of the Requirements for the Degree

Master of Mechanical Engineering

by

Sherman A. Clevenson

March 1952

AN EXPERIMENTAL AND ANALYTICAL INVESTIGATION OF THE FLUTTER AND DIVERGENCE OF LARGE MASSES AT THE ENDS OF SHORT STRUTS

A Thesis

Presented to

the Faculty of the Department of Engineering

University of Virginia

In Partial Fulfillment

of the Requirements for the Degree

Master of Mechanical Engineering

---

by

Sherman A. Clovenson

March 1952

APPROVAL SHEET

A thesis presented to the faculty of the Department of Engineering, University of Virginia, in partial fulfillment of the requirements for the Degree Master of Mechanical Engineering.

Sherman A. Clemson
Author

Charles E. Nielsen
Faculty Advisor

Subcommittee on Graduate Studies

TABLE OF CONTENTS

LIST OF TABLES

LIST OF FIGURES

CHAPTER I

THE PROBLEM AND HISTORICAL BACKGROUND

In this chapter the purpose of this experimental and analytical investigation of the flutter and divergence of large masses at the ends of short struts is given. A few remarks on the importance of this investigation follows. After a brief historical background, definitions of the terms and symbols used in this paper are given. The chapter is concluded with a summary of the organization of this paper.

Purpose of the investigation. The purpose of this investigation is to obtain experimental data on the flutter and divergence of large masses at the ends of short struts and to compare these data with corresponding analyses. Flutter is an oscillatory aeroelastic phenomenon which involves the interaction of aerodynamic, elastic, and inertia forces, and deals with the conditions whereby an aircraft component can extract energy from the surrounding air stream to an extent causing distortion or destruction. One type of flutter consists of a coupled bending-torsion oscillation. Another type of flutter consisting of a torsional instability single degree of freedom will be referred to as torsional instability in this paper. Divergence is the phenomenon in which the aerodynamic moment is greater than the structural restoring moment.

Importance of the problem. The problem of flutter and divergence of large masses at the ends of short struts has become of increasing importance. For example, such problems arise with wing tanks and jet engines suspended

from the wings of present-day high-speed aircraft, and with certain missile designs that have power plants consisting of ram jets outboard of the body. With such use of these large masses, investigations of flutter and divergence must be made so that precautionary measures may be taken.

Historical background. Until recent years there was little study of the problem of flutter or divergence of large masses at the ends of short struts. Innumerable investigations of wing flutter were made. As the airplane speed was increased and its configuration changed (wing tanks, etc.) investigations of flutter and divergence of wings with concentrated weights and aerodynamic shapes were made. These studies always concerned the combined effects of the wing and the shape. The present work is an attempt to isolate the aerodynamic effects of the shape. In order to do this experimentally, tests were made of various shaped bodies at the ends of short struts. These struts are so designed as to have negligible air forces on them.

Definition of terms and symbols. Flutter and divergence have already been defined in a previous section. The following is a list of symbols and their definitions which will be encountered in this paper. In order that a comparison may be made by designers with data in this paper, all parameters will be made nondimensional wherever practical. Figure 1 shows the physical significance of some of the parameters in the list of symbols.

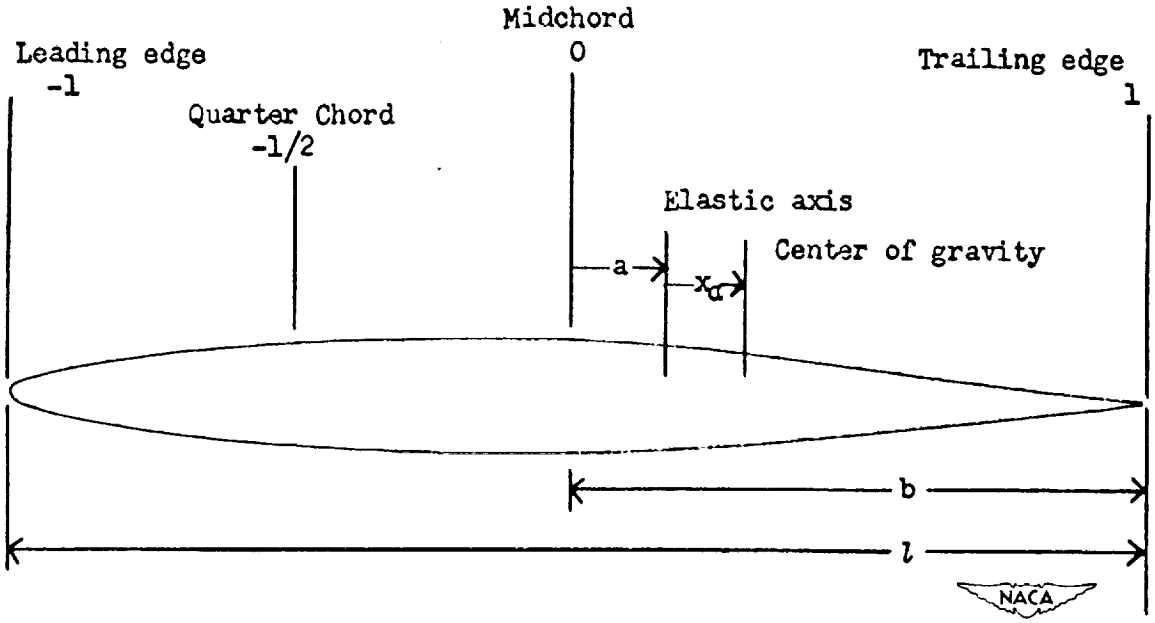

Figure 1.- Physical significance of some flutter parameters.

e.a.	elastic axis or axis of rotation position in percent chord measured from the leading edge of the basic configuration
a	nondimensional coordinate of axis of rotation from midchord $\left(\frac{2 \times \text{e.a.}}{100} - 1\right)$
c.g.	center-of-gravity position in percent chord measured from the leading edge of the basic configuration
x_α	location of the center of gravity measured from the e.a. and positive to the rear of the e.a. $\left(\frac{2 \times \text{c.g.}}{100} - 1 - a\right)$
ρ	density of test medium, slugs per cubic foot
ρ_o	standard density of dry air, slugs per cubic foot
q	dynamic pressure, pounds per square foot
M_o	Mach number
$M_{h\alpha}$	pitching moment, foot pounds
M	mass of body at ends of strut, pounds second squared per foot
$I_{e.a.}$	moment of inertia of the configuration about the elastic axis, inch pound seconds squared (I_α)
$2b = l$	length of basic body of revolution configuration, feet
g	damping coefficient
h	bending or translational deflection, inches
k_t	effective torsional spring constant, inch pounds per radian
k_b	effective bending spring constant, pounds per inch deflection
α	angle of attack, radians
ω	circular frequency, radians per second ($2\pi f$)
f_h	coupled natural bending frequency, cycles per second

f_α	coupled natural torsion frequency, cycles per second
f_t	frequency at which torsional instability occurs, cycles per second
f_f	frequency at which flutter occurs, cycles per second
v	speed, feet per second
v_f	flutter speed, feet per second
v_d	divergence speed, feet per second
v_t	torsional instability speed, feet per second
k	reduced frequency parameter ($b\omega/v$)
k_1	reduced frequency parameter ($l\omega/v$)
$L(x)$	total aerodynamic force $L(x) = P = F_h + F_\alpha$
F_h	aerodynamic force due to translation of the body
F_α	aerodynamic force due to rotation of the body
M_α	aerodynamic moment due to rotation of the body
M_h	aerodynamic moment due to translation of the body

Organization of paper. This paper will first present a brief review of other investigations of related problems. Following this review will be statements of the experimental methods of procedure and sources of data. The data will then be presented followed by an analytical investigation. After comparisons of the analytical results with the experimental data, this paper will be concluded with a summary and conclusions.

CHAPTER II

REVIEW OF RELATED STUDIES

In this chapter a review of related studies on the problem of flutter and divergence of large masses is given. Names of other investigators of related problems are also presented.

Related studies. As previously mentioned in the historical background, various investigations of flutter and divergence of wings with concentrated weights and aerodynamic shapes have been made. These studies are somewhat related to the present problem in that the wings may be considered as covered struts. However, in the previous investigations the masses of the weights were small compared to the mass of the wing. Also, the aerodynamic shapes had small surface areas compared to the surface area of the wing. Thus the aerodynamic forces on the wings were of much greater magnitude than those forces on the mass or shape at the end of the wing.

Other investigators of related problems. Runyan and Sewall[1] have made an extensive experimental investigation of the effects of concentrated weights on the flutter characteristics of a straight cantilever wing. The effects of aerodynamic shape of concentrated weights on the flutter speed of a straight cantilever wing were studied by Sewall and Woolston.[2] Both

---

[1] Harry L. Runyan and John L. Sewall, "Experimental Investigation of the Effects of Concentrated Weights on Flutter Characteristics of a Straight Cantilever Wing." NACA TN 1594, June, 1948.

[2] John L. Sewall and Donald S. Woolston, "Preliminary Experimental Investigation of the Aerodynamic Shape of Concentrated Weights on Flutter of a Straight Cantilever Wing." NACA RM L9E17, July, 1949.

studies concerned wing flutter and did not isolate the flutter of the mass or the shape by itself.

If the forces on the aerodynamic bodies were known, theoretical calculations could be made to determine whether flutter would occur. Munk[3] was one of the early investigators of the forces on aerodynamic shapes. His studies were theoretical and showed that for symmetrical bodies of revolution in steady state potential flow there would be no resultant lift force on the body. However, there would be a pitching moment. In a more recent paper, Allen of the NACA presents comparisons of analytically derived lift and moment coefficients for the steady case to experimental coefficients and showed excellent agreement. His analysis includes a term to account for the viscosity of the fluid, which results in a lift force where potential theory excludes it.

---

[3] M. M. Munk, "The Aerodynamic Forces on Airship Hulls." NACA Report 184.

CHAPTER III

METHODS OF PROCEDURE AND SOURCES OF DATA

In this chapter statements of the method of obtaining experimental flutter and divergence data utilizing a wind tunnel are made. The models and instrumentation are discussed. The sources of data are also given.

EXPERIMENTAL

Use of the 4.5 foot flutter tunnel. All tests were conducted in the 4.5-Foot Flutter Tunnel of the National Advisory Committee for Aeronautics. This tunnel is of the closed throat single return type employing air or Freon at variable pressures. All experiments reported herein were conducted in air. The top speed reported in these tests is 535 feet per second, or a Mach number equal to 0.48. The Reynolds number range was 1.5×10^6 to 7.1×10^6.

Models. For this investigation two basic configurations were used. The first model configuration was a body of revolution whose contour was an NACA 65020 airfoil section (Figure 2) mounted on struts. Its elastic axis position was varied by moving the body on the mounting struts. The struts consisted of two rods suspended vertically from the tunnel, one behind the other. The purpose of two rods was to give a high natural frequency in a fore and aft direction compared to the bending and torsion frequencies of the model configuration. Struts of various stiffnesses were used for both configurations.

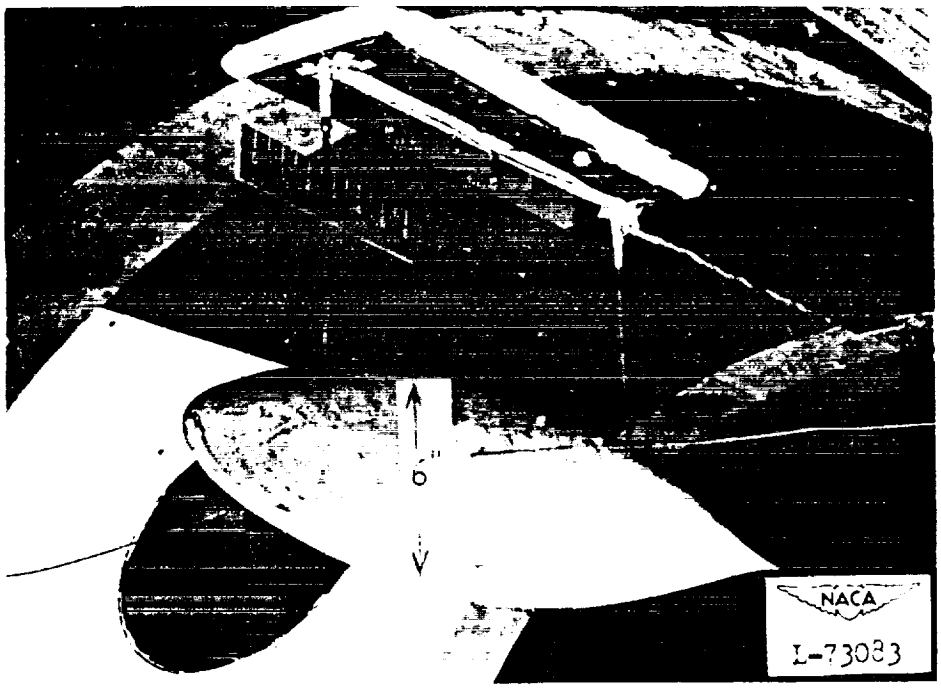

Configuration 1

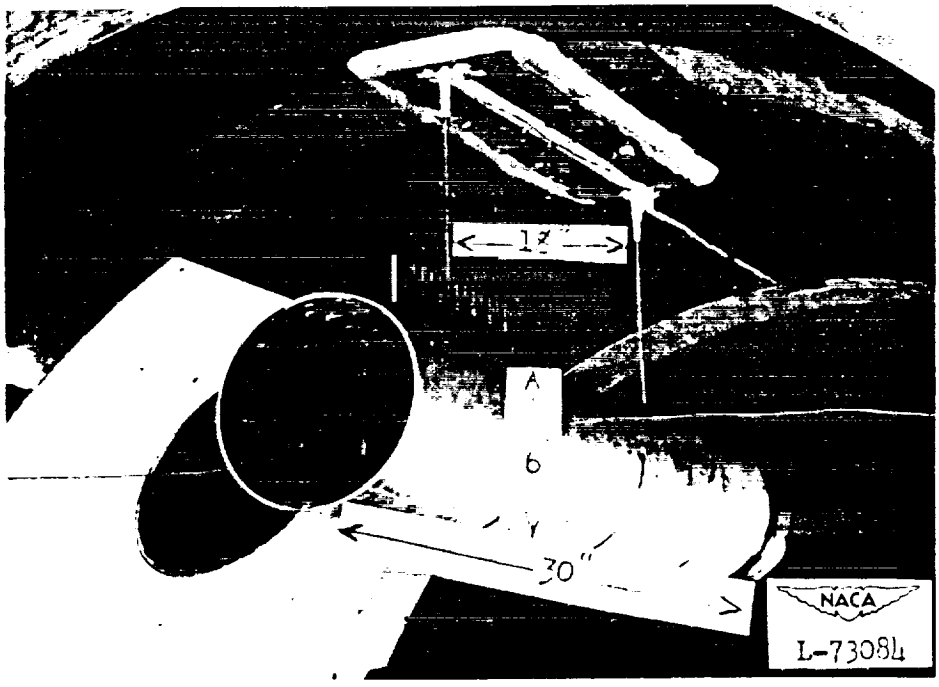

Configuration 2

Figure 2.- Dimensions of the two basic configurations and the test setup.

The second model consisted of a vented tube whose length to diameter ratio was the same as the airfoil-shaped body, namely thirty inches to six inches (Figure 2). Its weight and inertial properties were similar also. The center-of-gravity position could be varied by placing a flat ring inside the tube at various locations. The elastic axis position was changed by moving the tube on its supports, the supports remaining stationary.

Alterations to the second configuration were made by adding various shaped nose and rear sections (Figure 3) to the open tube thus changing the c.g., I_α, and body contour of the configuration.

Instrumentation. Electric resistance strain gages were glued to the roots of the supporting struts for measuring the strains due to bending deflections. By noting the phase between the bending of the forward strut and the bending of the rearward strut, the mode of oscillation was determined. The outputs of the strain gages were fed through amplifiers and into a multiple channel recording oscillograph.

Tunnel speeds were determined with the use of pressure recording instruments and then corrected with tunnel calibration correction factors.

EXPERIMENTAL DATA

Recordings. The chief source of data for this paper is the oscillograph recordings of the strain signals. From these permanent records, frequencies of oscillations were determined. The phasing of the recorded signals indicated the motion of the body.

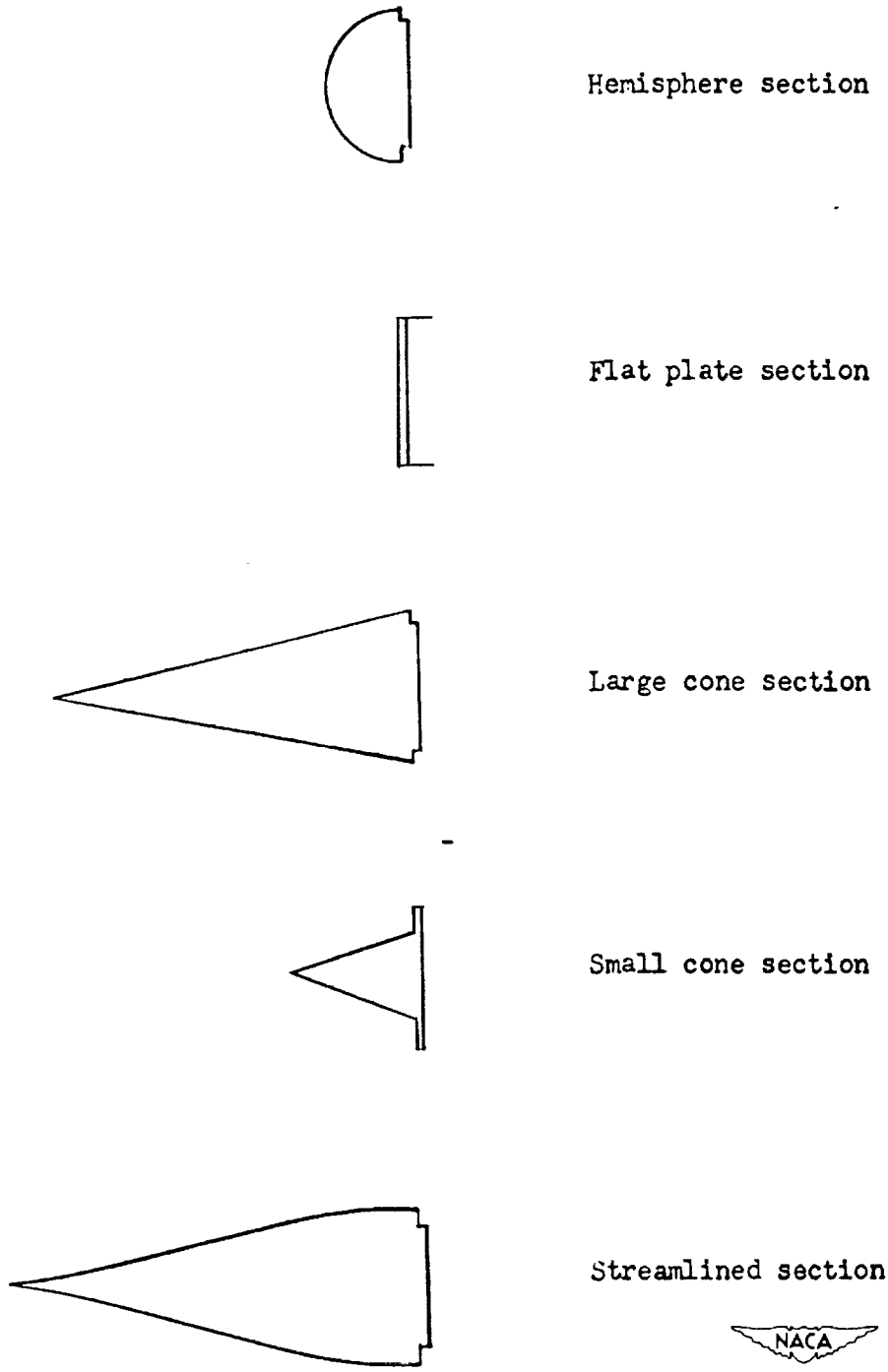

Figure 3.- Various nose and rear sections tested with the open tube.

Observations. In conjunction with all recordings, notes on observations were made. For example, when an oscillation occurred with increasing amplitude that appeared to be made up of both bending and torsion modes, it was called flutter. When no oscillation occurred, but the model started to twist and then translated (in the bending direction) over to the stops, it was called divergence. When the body underwent a sustained torsional oscillation with no apparent translation and with no tendency for the amplitude of this oscillation to increase to destructive proportions, it was called torsional instability.

CHAPTER IV

PRESENTATION AND DISCUSSION OF DATA

This chapter deals with the presentation and discussion of data for three phenomena; flutter, divergence, and torsional instability.

FLUTTER

Effect of density. Flutter was obtained on both basic configurations. After obtaining the phenomenon by using sufficiently weak struts, the effect of density of the test medium on the flutter speed and flutter frequency was studied. These speeds, frequencies, and densities are plotted (Figures 4-7) as nondimensional coefficients. Figure 4 shows the variation of flutter speed with density for the airfoil-shaped body. It may be seen in Figure 4 that the flutter speed coefficient $\frac{V_f}{b\omega_\alpha}$ of the body with the airfoil section increases with decreasing density. (An increase in altitude at which an aircraft is flying may be interpreted as a decrease in density.) This flutter speed coefficient represents the speed at which an oscillation composed of both bending and torsion, not in phase with each other, could be seen. In general, at flutter the amplitude of the oscillation increased with no increase in tunnel speed. The usual practice was to reduce the tunnel speed as quickly as possible at the onset of flutter to prevent possible destruction of the model.

Figure 5 shows the variation of flutter frequency with density for the airfoil-shaped body. There appeared to be little variation in the flutter frequency parameter $\frac{f_f}{f_\alpha}$ of the airfoil-shaped body as the density was changed. This would indicate that in this speed range the

flutter frequency of the closed body configuration would remain essentially constant and independent of the flutter speed.

Figure 6 shows the variation of flutter speed with density for the open tube configuration. In Figure 6 the flutter speed coefficient for the open tube is seen to increase as the density decreases. This coefficient is lower than the corresponding coefficient of the airfoil-shaped body as seen by comparing Figure 6 with Figure 4. Figure 7 shows the variation of flutter frequency with density for the open tube configuration. A comparison of Figure 7 with Figure 5 shows that the flutter frequency of the open tube is somewhat higher than the corresponding parameter for the airfoil-shaped body. For ease in comparing values of the two configurations and to show other parameters, Tables I and II are presented.

Effect of center-of-gravity location. The results of a series of tests in which movable weights were used to vary the center-of-gravity position of the vented tube are given in Table III and shown in Figures 8 and 9. These changes affected the mass, inertia, and frequency parameters. It may be seen from Figures 8 and 9 that when x_α, the nondimensional center-of-gravity location, was positive, flutter was encountered, and when x_α was negative, divergence occurred. A similar trend concerning flutter and divergence depending on the relative position of the elastic axis and center-of-gravity positions, for wings alone, was shown theoretically in a simplified flutter speed formula by Theodorsen.[4]

---

[4] T. Theordorsen, "General Theory of Aerodynamic Instability and the Mechanism of Flutter." NACA Report 496.

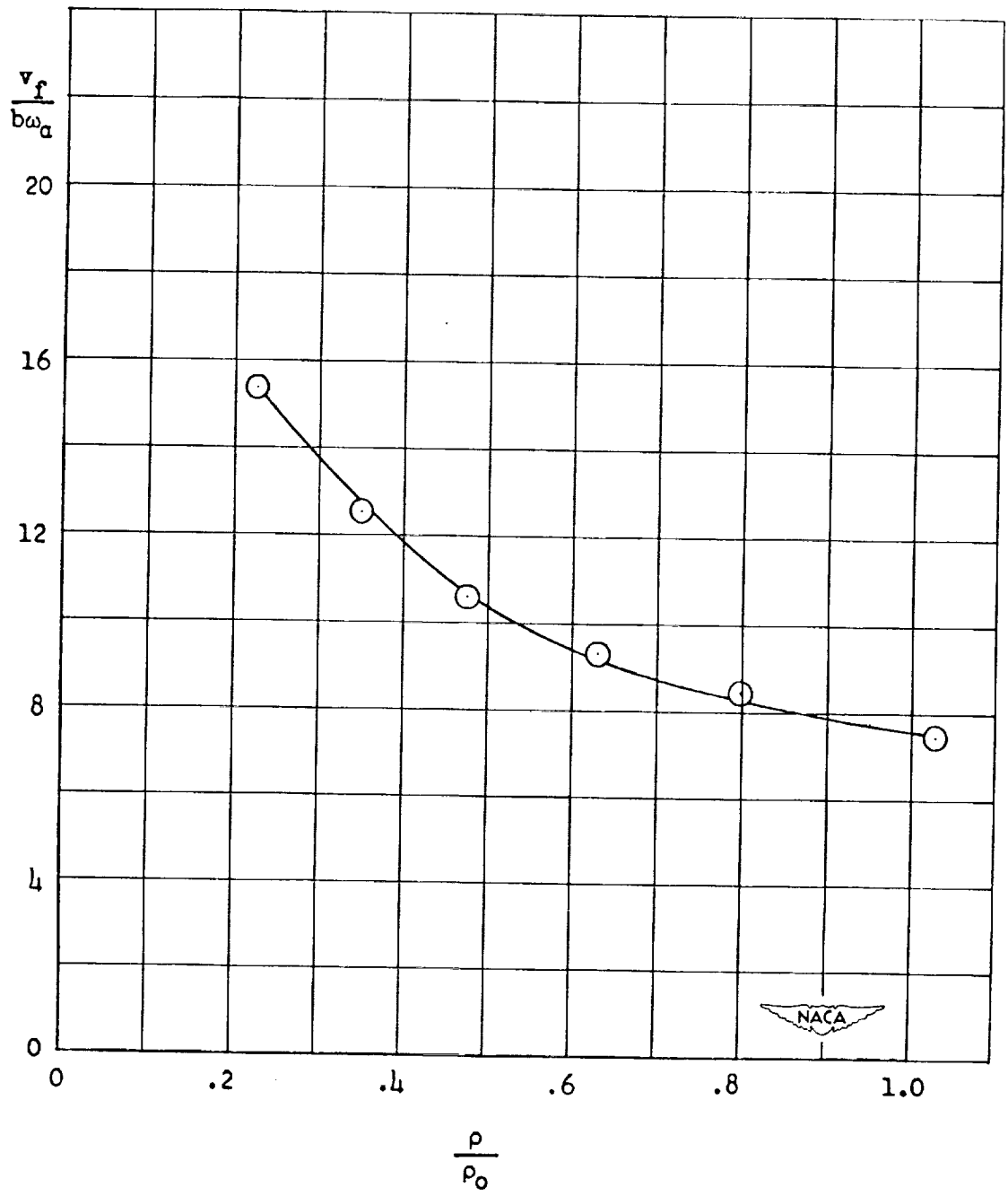

Figure 4.- Variation of flutter speed coefficient with density coefficient for the airfoil-shaped body.

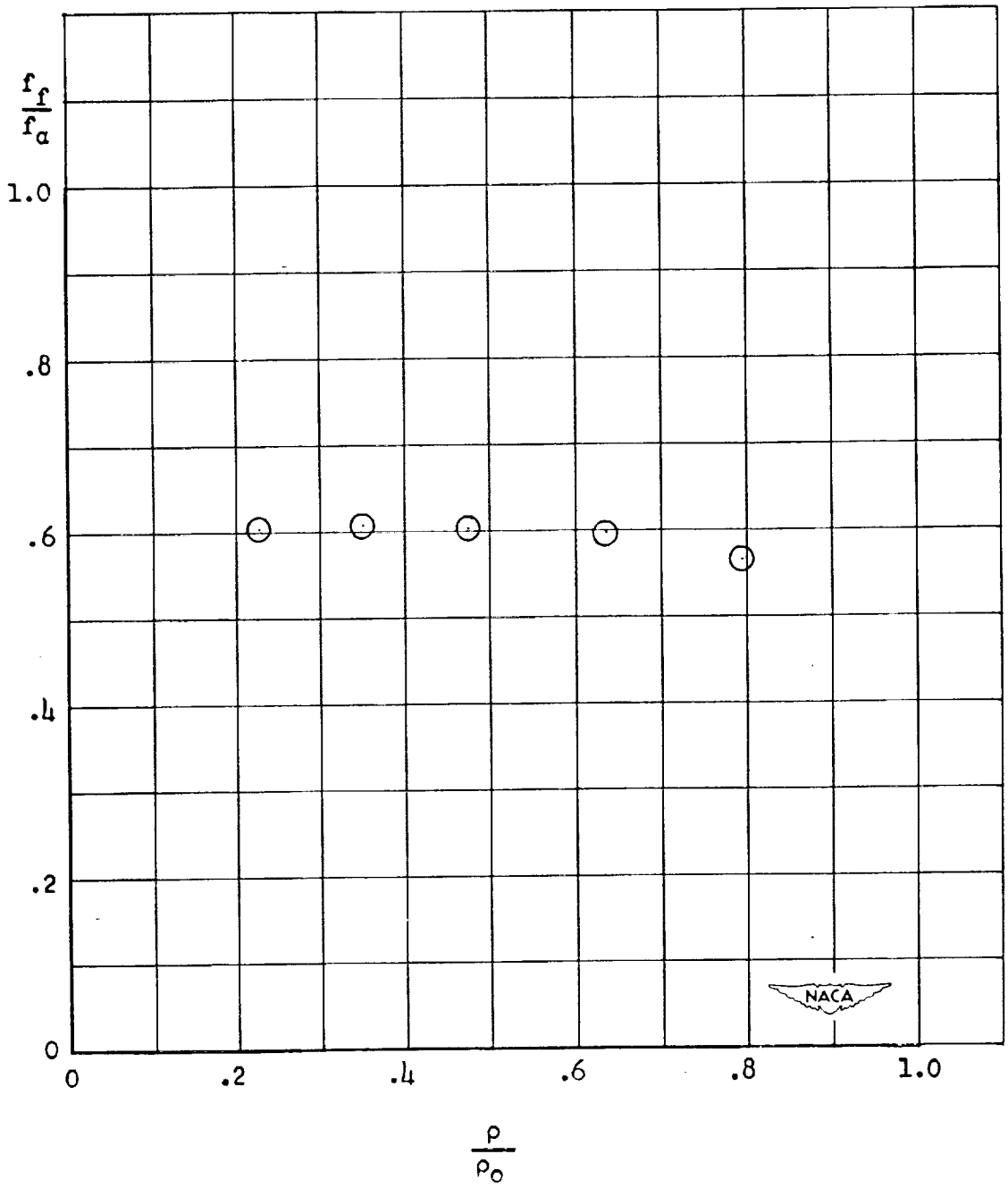

Figure 5.- Variation of flutter frequency coefficient with density coefficient for the airfoil-shaped body.

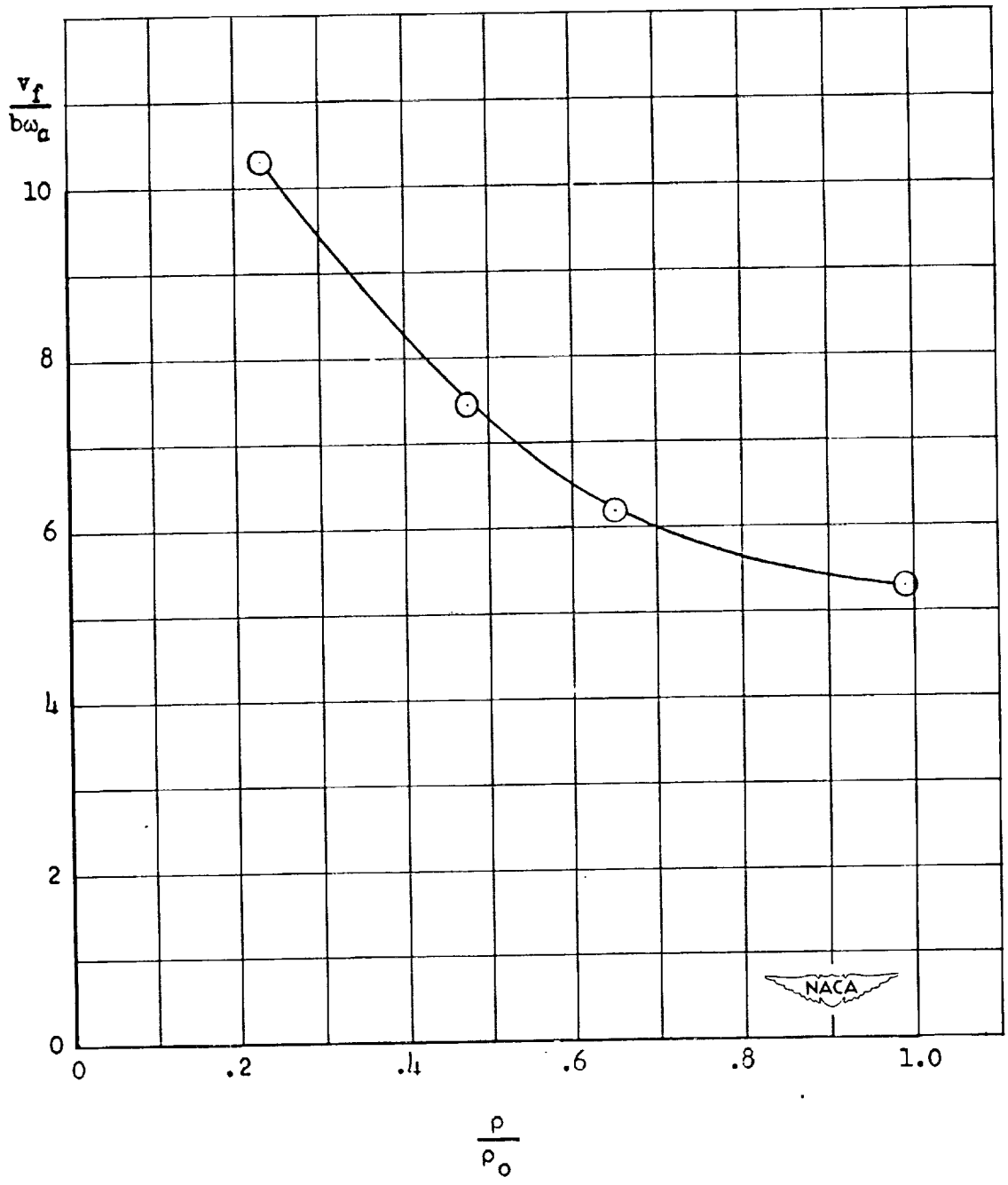

Figure 6.- Variation of flutter speed coefficient with density coefficient for the open-tube configuration.

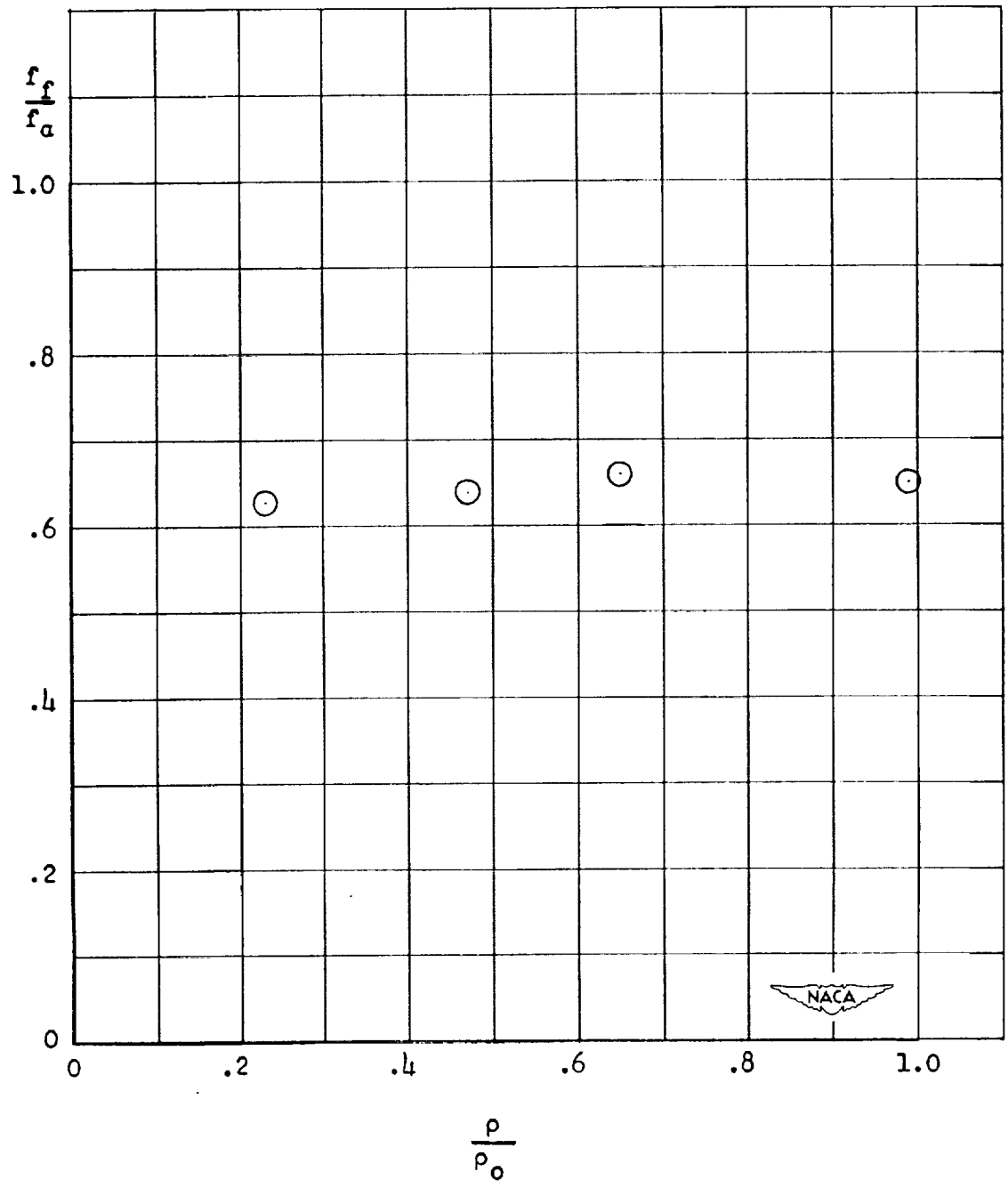

Figure 7.- Variation of flutter frequency coefficient with density coefficient for the open-tube configuration.

TABLE I

EFFECT OF DENSITY ON THE AIRFOIL-SHAPED BODY OF REVOLUTIONS

f_f	f_f/f_α		v_f	$v_f/b\omega_\alpha$		$\rho \times 10^{-2}$	ρ/ρ_o	x_α	a
Exp.	Exp.	Ana.	Exp.	Exp.	Ana.				
1.70	0.603	*	341	15.39	*	0.054	0.227	-0.10	-0.08
1.75	.621	*	277	12.51	*	.083	.349	-.10	-.08
1.71	.606	*	235	10.62	*	.113	.475	-.10	-.08
1.69	.599	*	207	9.34	*	.150	.631	-.10	-.08
1.60	.567	*	187	8.42	*	.190	.799	-.10	-.08
- -	- - -	*	172	7.76	*	.250	1.051	-.10	-.08

*no solution $f_h = 1.20$ $f_\alpha = 2.82$ $I_\alpha = 0.0690$ $M = 0.1301$

TABLE II

EFFECT OF DENSITY ON THE OPEN TUBE CONFIGURATION

f_f	f_f/f_α		v_f	$v_f/b\omega_\alpha$		$\rho \times 10^{-2}$	ρ/ρ_o	x_α	a
Exp.	Exp.	Ana.		Exp.	Ana.				
1.51	0.629	0.85	195	10.32	10.16	0.055	0.231	0.14	∞
1.54	.642	.84	147	7.46	6.22	.112	.471	.14	∞
1.58	.658	.93	117	6.19	4.91	.155	.652	.14	∞
1.56	.650	.94	100	5.30	3.71	.235	.988	.14	∞

$M = 0.1410$ $f_h = 1.37$ $f_\alpha = 2.40$ $I_\alpha = 0.0864$

TABLE III

FLUTTER AND DIVERGENCE OF THE VENTED TUBE WITH THE CENTER-OF-GRAVITY POSITION VARIED BY MOVING WEIGHTS

x_a	a	M	I_a	f_f Exp.	$\frac{f_f}{f_a}$ Exp.	$\frac{f_f}{f_a}$ Ana.	f_a	f_h	ρ/ρ_o	$\frac{v_f}{b\omega_a}$ Exp.	$\frac{v_f}{b\omega_a}$ Ana.	$\frac{v_d}{b\omega_a}$ Exp.
0.08	0	0.1410	0.0875	*	*	0.76	8.4	3.10	0.90	5.71	6.35	- -
.00	0	.1410	.0708	diverge		.65	9.2	3.11	.90	- -	7.10	5.47
.14	0	.1410	.0957	5.50	0.67	.78	8.2	3.07	.90	5.73	5.43	- -
.26	0	.1580	.1217	*	*	.95	7.41	3.01	.90	6.06	5.04	- -
.36	0	.1750	.1475	4.60	.65	1.06	7.04	2.81	.90	6.00	4.79	- -
.00	0	.1580	.1217	*	*	.71	7.3	3.00	.90	6.78	8.63	- -
-.14	0	.1750	.1475	diverge		.64	6.8	2.83	.90	- -	11.82	7.95
-.26	0	.1580	.1217	diverge		.53	7.5	2.96	.90	- -	17.37	6.37

*Not obtained

TABLE III - (Continued)

x_a	$\frac{v_d}{b\omega_a}$ Ana.	v_f Exp.	v_f Ana.	v_d Exp.	v_d Ana.	M_o Exp.
0.08	10.2	377	420	- -	671	0.33
.00	9.3	- -	513	396	671	.35
.14	10.4	369	350	- -	671	.32
.26	11.5	353	293	- -	671	.31
.36	12.1	331	265	- -	671	.29
.00	11.7	389	495	- -	671	.34
-.14	12.6	- -	635	424	671	.37
-.26	11.4	- -	1022	375	671	.34

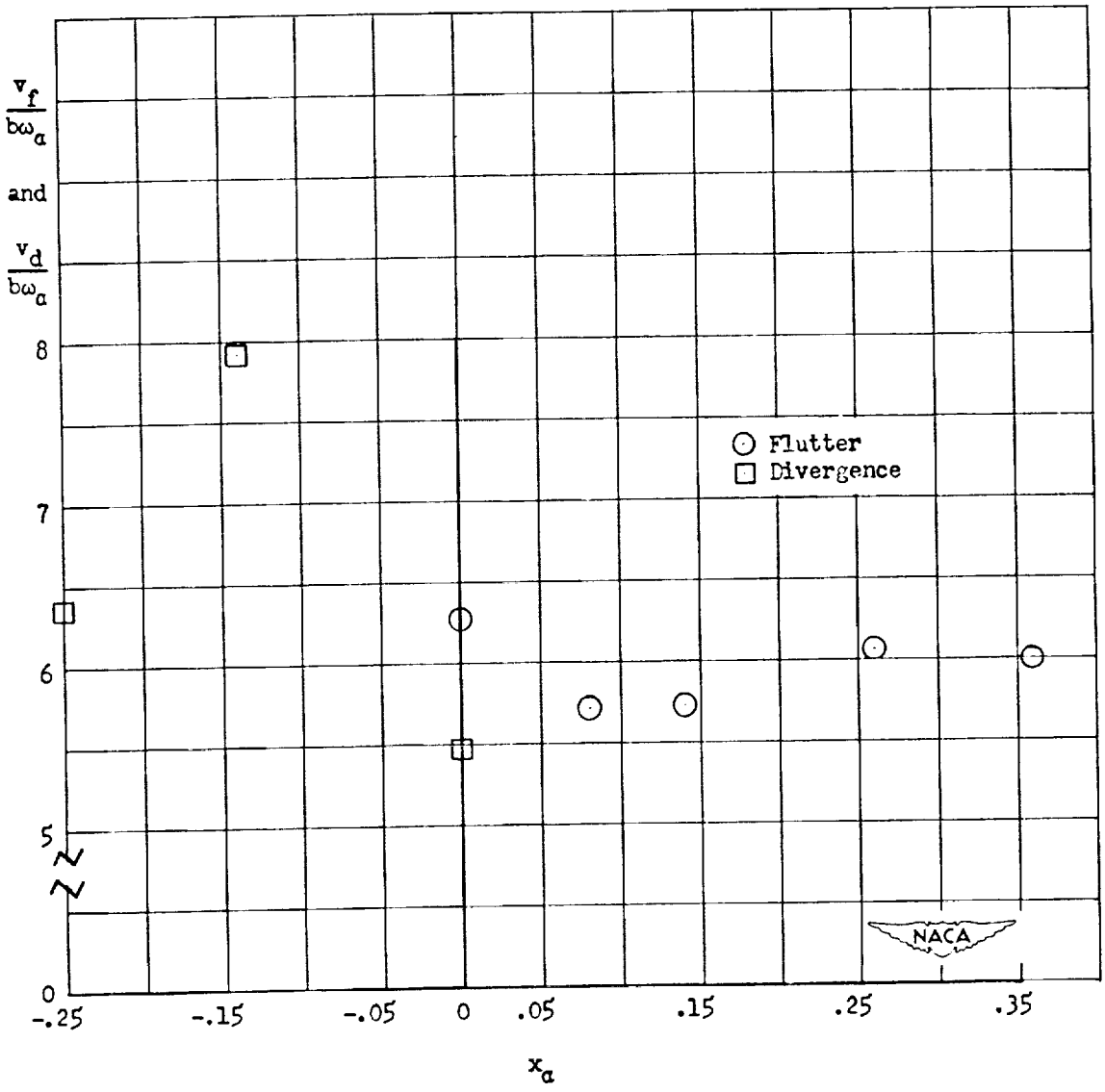

Figure 8.- Variation of flutter speed and divergence speed coefficients with nondimensional center-of-gravity position x_α for the open-tube configuration.

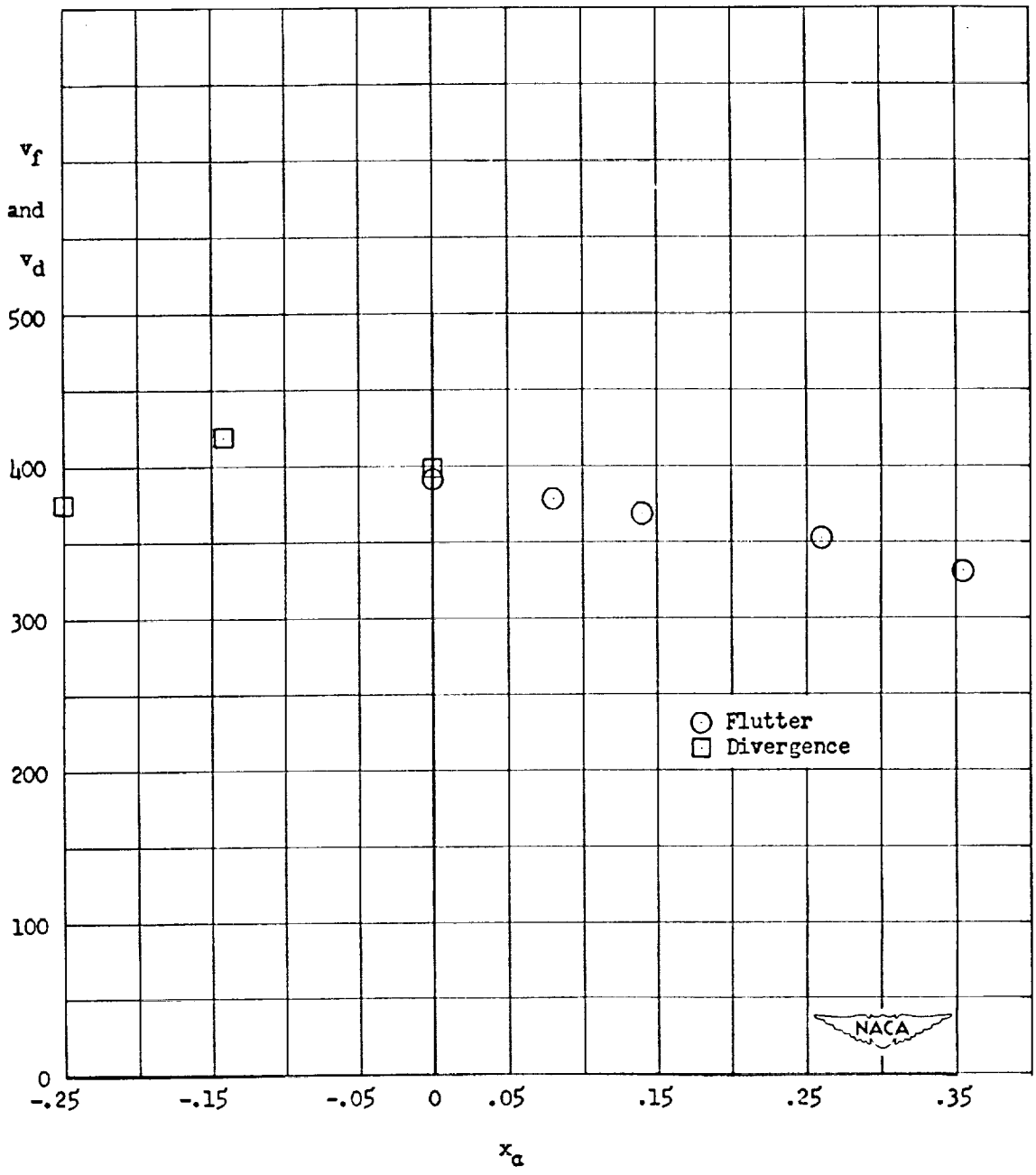

Figure 9.- Variation of flutter speed and divergence speed with nondimensional center-of-gravity position for the open-tube configuration.

The flutter speed coefficient $\frac{V_f}{b\omega_\alpha}$ is essentially independent of the center-of-gravity location (Figure 8) for positive values of x_α when the center-of-gravity position is varied as in these tests. As previously mentioned, the location of weights determined the center-of-gravity position and also changed the natural frequencies of the system. As the center-of-gravity position was located further from the midchord, the torsional frequency ω_α decreased. Thus, for the flutter speed coefficient to remain essentially constant, the actual flutter speed decreased. This decrease is shown in Figure 9. It would appear beneficial from a flutter standpoint to have the center-of-gravity position at least as far forward as the axis of rotation. When the center-of-gravity position is located ahead of the axis of rotation other phenomena may become critical.

DIVERGENCE

Divergence speeds of the airfoil shaped body were not determined in this investigation. Random bending and torsional oscillations of the configuration using a weak set of struts limited the test speeds to low values. Using a stiffer set of struts, divergence was not obtained for velocities in the range of the experiment (M_o up to 0.48). However, the divergence phenomena for the vented tube was obtained experimentally. Divergence speed coefficients for the vented tube are shown in Figure 8. The divergence speed was obtained by holding the tube as close to zero angle of attack as possible and increasing the airspeed in the tunnel until the model translated to the stops. If conditions were such that flutter occurred first, a divergence speed was not obtained. Theory of wing

divergence indicates the divergence speed to be independent of c.g. position. It might be expected for the open tube divergence speeds to be independent of c.g. location, also. However, the divergence speed coefficient would not be expected to remain constant since the inertia, and consequently the base frequency ω_α was varied. The actual divergence speeds are shown in Figure 9. The scatter in the data might possibly be attributed to testing techniques, or to a mass-ratio effect (mass of tube to mass of surrounding air), or tunnal roughness. No divergence was obtained for the aft locations of the center-of-gravity position since flutter conditions were encountered prior to divergence. However, where divergence was encountered, the data suggest that the divergence speed is independent of center-of-gravity location.

With stronger struts, no divergence speeds were obtained within the limits of the test speeds encountered. When certain of the nose and rear sections were placed on the tube, a single degree-of-freedom torsional instability occurred. No divergence speeds were obtained for these configurations.

TORSIONAL INSTABILITY FLUTTER

Torsional instability flutter is differentiated from flutter in that the former refers to a single degree of freedom, usually an oscillation about the axis of rotation, and the later refers to a coupled oscillation wherein two or more degrees of freedom are involved. Torsional instability was obtained on both configurations in this investigation.

Torsional instability of the airfoil-shaped body. The torsional oscillation of the airfoil-shaped body was observed to have greater amplitude of motion for higher airspeeds. However, destructive amplitudes were not encountered. Figure 10 shows the variation of the instability frequency with airspeed for the airfoil-shaped body. The frequency of oscillation was seen to decrease as the airspeed was increased (shown also in Table IV).

Torsional instability of the vented tube. No torsional instability of the vented tube was encountered in these series of tests.

Torsional instability of the closed tube. A decrease in instability frequency was found for the configurations of the tube which exhibited the torsional instability. The amplitude of motion was also found to increase with increasing airspeed. Table V is a listing of the different configurations tested to obtain flutter data. Under the heading M_o is the Mach number range in which the oscillation occurred, or the maximum Mach number of the particular test. Under the heading f_t are the torsional instability frequency ranges for that test. The configuration columns indicate which section was used at the front and rear of the tube. It may be noted that all the configurations with a hemisphere rear section exhibited the instability whereas a blunt rear section (cover plate) had a tendency to eliminate this instability. Elimination of the instability was also obtained when using a large streamlined body for the rear section.

A study of the effect of density on the configuration with the hemisphere nose and hemisphere rear sections was made.

TABLE IV

EFFECT OF AIRSPEED ON THE INSTABILITY FREQUENCY OF THE AIRFOIL-SHAPED BODY

f_t	$f_{t_{Ana.}}$	f_t/f_α	v_t	$\frac{v_t}{b\omega_\alpha}$	ρ/ρ_o	x_α	a
9.25	9.13	0.916	299	3.76	0.98	0	-0.18
8.95	8.95	.883	340	4.29	.97	0	.18
8.77	8.50	.868	387	4.88	.96	0	.18
8.47	8.13	.839	443	5.58	.95	0	.18
8.06	7.57	.748	505	6.30	.93	0	.18
7.75	7.18	.767	532	6.70	.92	0	.18

$M = 0.1300$ $f_h = 4.00$ $f_\alpha = 10.1$ $I_\alpha = 0.0670$

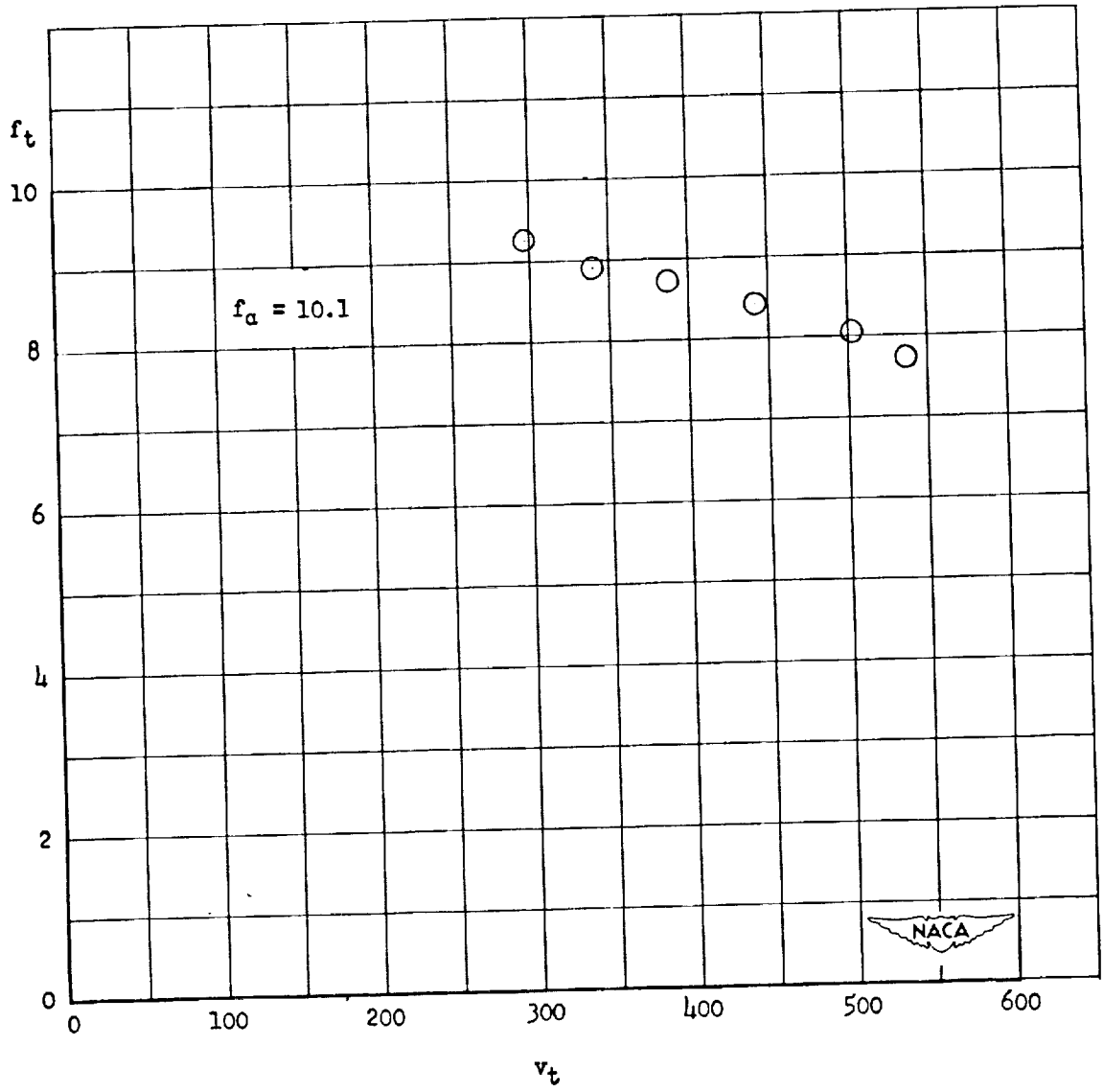

Figure 10.- Variation of instability frequency with airspeed for the airfoil-shaped body.

TABLE V

TUBE CONFIGURATIONS INVESTIGATED FOR TORSIONAL INSTABILITY

Test	M_o	c.g.	e.a.	k_b	k_t	f_h	f_a	f_t
1	0.48	50	50	16.9	9742	6.43	17.5	- - - - -
2	0.20-0.24	50	40	16.9	9742	5.85	14.4	14.1-13.9
3	0.48	48	40	16.9	9742	5.85	14.4	- - - - -
4	0.35	50	40	16.9	9742	5.91	14.4	- - - - -
5	0.43	53	40	16.9	9742	5.61	12.9	- - - - -
6	0.21-0.27	53	50	8.7	5095	4.18	9.2	8.58-8.34
7	0.14-0.20	50	62	8.7	5095	4.03	10.2	10.3-10.1
8	0.28-0.37	48	50	8.7	5095	4.34	10.9	- - - - -
9	0.22-0.38	62	50	8.7	5095	3.96	8.0	6.15
10	0.39	62	72	8.7	5095	4.11	7.5	- - - - -
11	0.21	50	28	4.2	2965	3.08	7.9	7.70-7.50
12	0.29	50	50	4.2	2965	3.92	10.1	- - - - -
13	0.20-0.23	48	40	16.9	9742	5.86	14.7	14.7
14	0.47	50	40	16.9	9742	5.87	14.9	- - - - -
15	0.20-0.23	50	40	16.9	9742	5.90	14.8	14.7-14.5
16	0.33	55	40	16.9	9742	5.65	13.2	- - - - -
17	0.19-0.27	64	50	8.7	5095	3.92	8.1	7.8
18	0.38	37	50	8.7	5095	4.00	8.0	- - - - -
19	0.14-0.23	38	50	8.7	5095	3.92	7.8	7.5-7.4
20	0.43	41	50	8.7	5095	3.16	7.2	- - - - -

TABLE V - (Continued)

Test	Configuration		Remarks
	Nose	Rear	
1	None	None	Nothing
2	Hemisphere	Hemisphere	Instability
3	Hemisphere	Cover plate	Nothing
4	Hemisphere	Small cone	Nothing
5	Hemisphere	Large cone	Nothing
6	Hemisphere	Large cone	Instability
7	Hemisphere	Hemisphere	Instability
8	Hemisphere	Cover plate	Intermittent instability
9	Hemisphere	Streamlined	Intermittent instability
10	Hemisphere	Streamlined	Intermittent instability
11	Hemisphere	Hemisphere	Instability
12	None	None	Nothing
13	Cover plate	Hemisphere	Instability
14	Cover plate	Cover plate	Nothing
15	Small cone	Hemisphere	Instability
16	Small cone	Large cone	Nothing
17	Cover plate	Streamlined	Intermittent instability
18	Streamlined	Cover plate	Nothing
19	Streamlined	Hemisphere	Instability
20	Streamlined	Large cone	Nothing

Figure 11 shows the variation of instability speed with density for the vented tube configuration with the hemisphere nose and rear sections. It is shown in Figure 11 and in Table VI that the instability speed coefficient $\frac{V_t}{b\omega_\alpha}$ increased slowly from standard density to about one-half standard density. Then as the density decreased, the instability speed coefficient increased rather rapidly. Figure 12 shows the variation of the instability frequency with density for the vented tube configuration with the hemisphere nose and rear sections. It may be seen that the instability frequency remained essentially constant at approximately the natural frequency of the configuration. These same trends of an increase of flutter speed coefficient with decreasing density and constant torsional instability frequency with density were shown in Figures 4 through 7 for the flutter of both the airfoil shaped body and the vented tube.

TABLE VI

EFFECT OF DENSITY ON THE INSTABILITY SPEED

OF THE OPEN TUBE CONFIGURATION

f_t	f_t/f_α	v_t	$\frac{v_t}{b\omega_\alpha}$	$\rho \times 10^{-2}$	ρ/ρ_o	x_α	a
10.5	0.99	423	5.07	0.023	0.097	0	0
10.7	1.01	314	3.78	.042	.177	0	0
10.5	.99	233	2.80	.061	.257	0	0
10.7	1.01	194	2.34	.080	.336	0	0
10.4	.98	171	2.05	.099	.416	0	0
10.7	1.01	160	1.92	.119	.500	0	0
10.7	1.01	160	1.92	.138	.580	0	0
10.7	1.01	162	1.94	.157	.660	0	0
10.6	1.00	152	1.82	.177	.744	0	0
10.6	1.00	158	1.90	.196	.824	0	0
10.6	1.00	145	1.74	.215	.904	0	0
10.4	.98	129	1.55	.231	.971	0	0

$\mu = 0.1375$ $f_h = 4.35$ $f_\alpha = 10.6$ $I_\alpha = 0.1031$

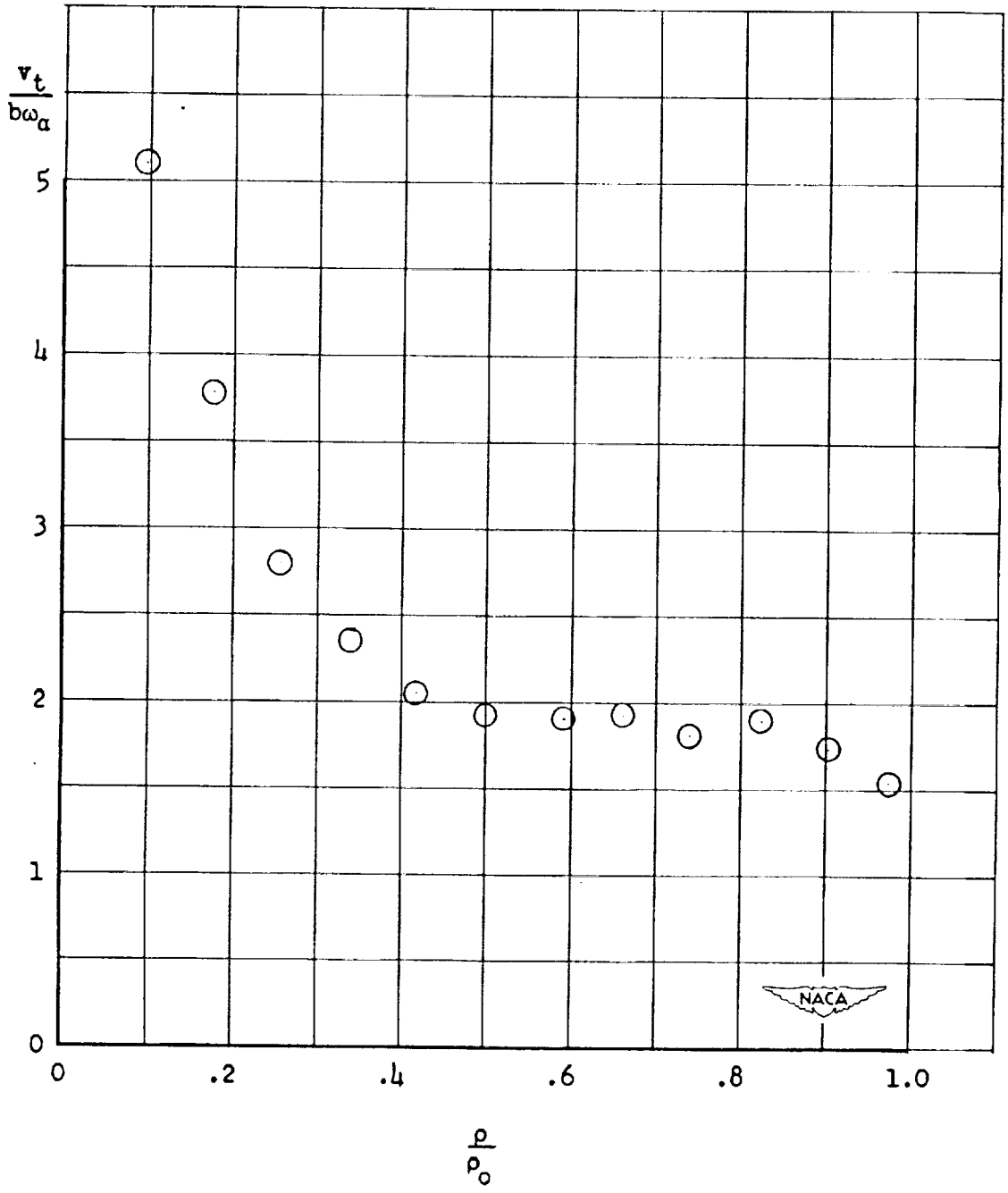

Figure 11.- Variation of instability speed coefficient with density coefficient for the tube configuration with hemisphere nose and rear sections.

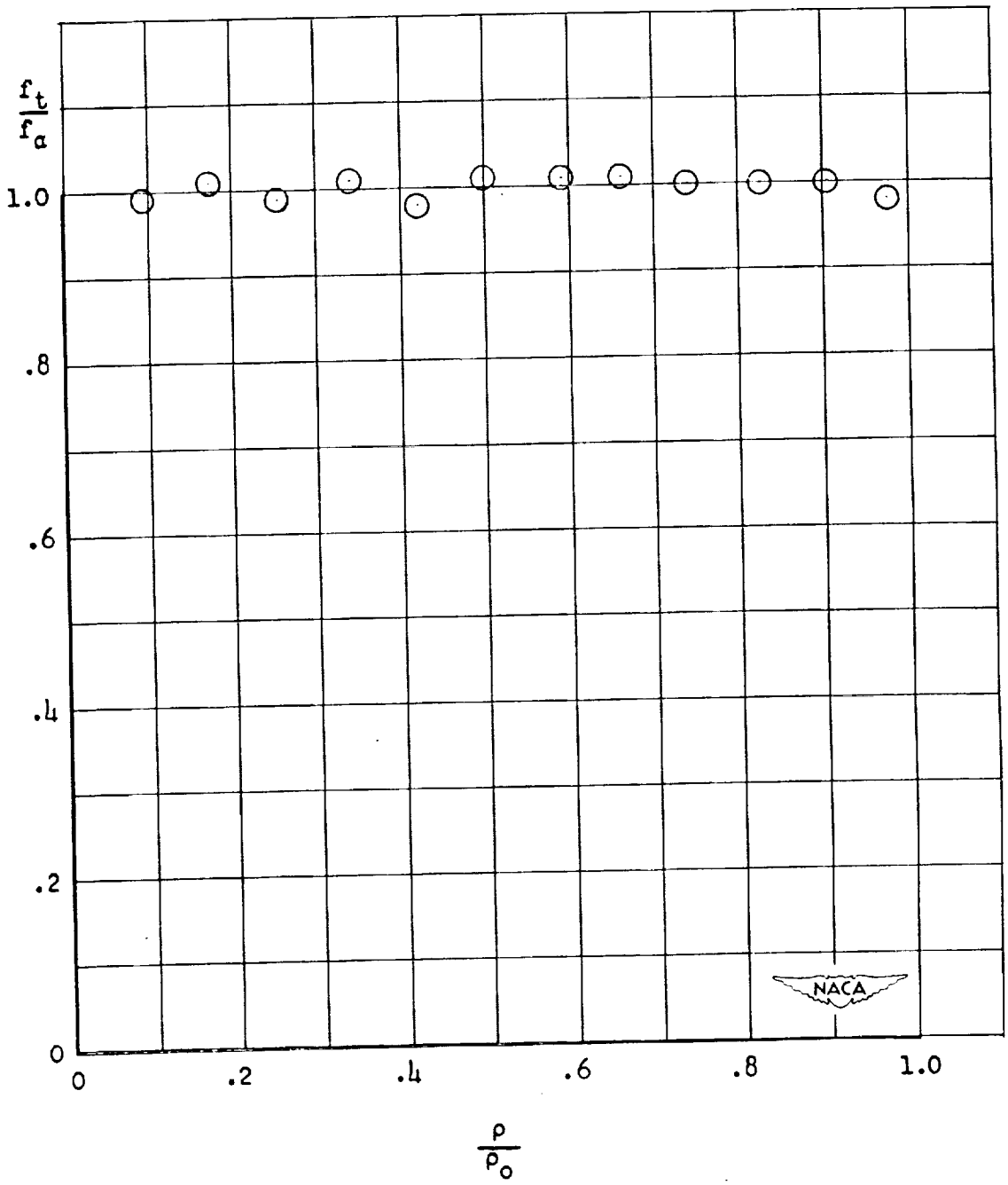

Figure 12.- Variation of frequency coefficient with density coefficient for the tube configuration with hemisphere nose and rear sections.

CHAPTER V

ANALYTICAL INVESTIGATION

Analytical investigations based on the meager amount of existing data are carried out for the three phenomena for which data was presented in the preceding chapter, namely, flutter, divergence, and torsional instability.

FLUTTER

As previously defined, flutter is an oscillatory aeroelastic phenomenon involving the interaction of the aerodynamic, inertia, and elastic forces. For both configurations the motion was observed to be a coupled oscillation which involved a rotation and a translation of the body. For this type of motion, the differential equations that govern the motion are as follows:

$$\text{For torsion:} \quad -I_\alpha \ddot{\alpha} - S_\alpha \ddot{h} - C_\alpha \alpha + M_{h\alpha} = 0 \tag{1}$$

$$\text{For translation:} \quad -S_\alpha \ddot{\alpha} - M\ddot{h} - C_h h + F_A = 0 \tag{2}$$

The forces and moments acting on the closed body are illustrated in Figure 13, where $S_\alpha = Mz$ and is positive when the c.g. is behind the e.a., and the dot denotes derivative with respect to time.

The physical parameters directly related to the body (mass, spring constant, e.a., c.g., etc.) are obtained from measurements. However, the external aerodynamic forces, are, for the most part redundant, there being a lack of experimental evidence as to their quantitative nature. In general, there are two categories of forces; on the one hand, those forces

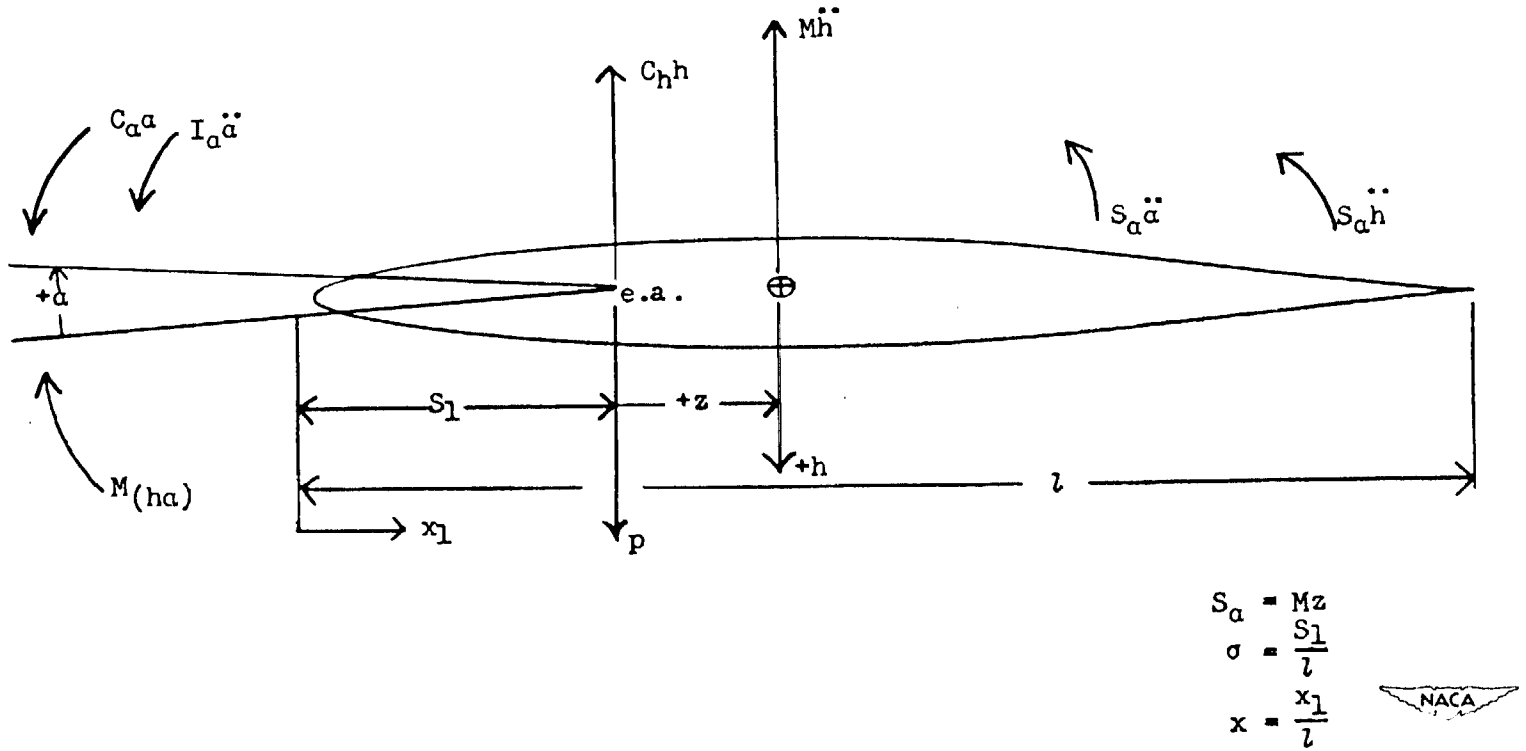

Figure 13.- Forces and moments acting on a closed body of revolution.

that may be represented by potential flow theory, and on the other hand, those forces associated with viscosity effects. In the following analysis, only those forces given by potential flow theory will be considered.

Flutter of the airfoil-shaped body of revolution. Work on the application of potential flow theory to bodies of revolution for the dynamic case has been done by Miles[5] and others. His solution for the forces on bodies of revolution will be adapted and employed for this analysis of a closed body. For the incompressible case, Miles gives for the velocity potential for a slender body of revolution undergoing harmonic motion

$$\phi(x, r, \theta, \tau) = w(x)R^2(x) \frac{\cos \theta}{r} e^{ik_1\tau} \tag{3}$$

where x, r, θ, are nondimensional polar coordinates of the system and

$\tau = \frac{Ut}{l}$

U = velocity (corresponds to v)

t = time

l = length of body, feet

$w(x)$ = local vertical velocity

$R(x)$ = radius of cross section of body of revolution at station x

M = mass of body, pounds second squared per foot

$k_1 = \frac{k\omega}{U}$

ω = circular frequency, radians per second

$k_1\tau = \omega t$

---

[5] J. W. Miles, "On Non-Steady Motion of Slender Bodies." Aeronautical Quarterly, Vol. II, Part 3, November, 1950.

This potential is subject to the conditions given by Lin, Reissner, and Tsien[6] for the validity of the linearization which are that the Mach number times the slenderness ratio is much less than one and that the Mach number times the slenderness ratio times the reduced frequency ratio $\frac{k\omega}{V}$ is much less than one, namely

$$M_o\delta \ll 1$$

and

$$M_o\delta k_1 \ll 1$$

where

$$\frac{k\omega}{V} = k_1$$

and

δ = slenderness ratio (diameter divided by length)

The pressure on the body may be evaluated at any point by means of the linearized Bernouilli equation.

$$\text{pressure} = -\rho \frac{D\phi}{Dt} = -\rho U\left(\frac{\partial \phi}{\partial x} + ik_1\phi\right) \tag{4}$$

If $m(x)$ is the virtual mass of a cross section at x, the local transverse force may be calculated directly from Newton's law, namely,

$$\frac{\partial}{\partial x} L(x) = \frac{D}{Dt}\left[m(x)w(x)e^{i\omega t}\right] \tag{5}$$

---

[6] C. C. Lin, E. Reissner, and H. S. Tsien, "On Two-Dimensional Non-Steady Motion of a Slender Body in a Compressible Fluid." Journal of Mathematics and Physics, 27, pp. 220-231, October, 1948.

Since for a body of revolution $m = \pi\rho R^2(x)$

$$\frac{\partial L(x)}{\partial x} = U\left(\frac{\partial}{\partial x} + ik_1\right)\left[\pi\rho R^2(x)w(x)\right] e^{i\omega t} \tag{6}$$

where

$$L(x) = F_A = F_\alpha + F_h \tag{7}$$

The aerodynamic moment is obtained by multiplying the incremental F_A by its lever arm to the axis of rotation. The moment is composed of both the moments due to rotation and translation. Thus

$$M_{h\alpha} = M_\alpha + M_h \tag{8}$$

Various operations will be performed on equation (6) so that the forces and moments due to translation and rotation of the body may be determined. Two equations of motion in terms of angle of attack (α) and translation (h) with two unknowns, flutter speed and frequency, will be obtained. The determinant to give other than a trivial solution will be shown.

Multiplying and dividing equation (6) by U and integrating over the nondimensional length of the body, the following expression is obtained for the force due to torsional oscillation:

$$F_\alpha = -l^2 \int_0^1 \rho U^2\left(\frac{\partial}{\partial x} + ik_1\right)\left[S(x)\,\frac{w(x)}{U}\right] e^{i\omega t}\,dx \tag{9}$$

where

$$S(x) = \pi\left(\frac{R}{l}\right)^2 \quad \text{at station } x$$

$$x = \frac{x_1}{l} \quad \text{nondimensional distance in } x \text{ direction}$$

$\sigma = \frac{S_1}{l}$ nondimensional distance to the axis of rotation (same as e.a.)

$$\frac{w(x)}{U} = +\frac{U\alpha}{U}\left[1 + ik_1(x - \sigma)\right]$$

$$\frac{1}{U}\frac{\partial w(x)}{\partial x} = + \frac{iU\alpha k_1}{U}$$

Simplifying equation (9) gives

$$F_\alpha = -\rho U^2 l^2 \int_0^1 \left\{\frac{\partial S(x)}{\partial x}\alpha\left[1 + ik_1(x - \sigma)\right] + S(x)ik_1\alpha + ik_1\alpha S(x)\left[1 + ik_1(x - \sigma)\right]\right\}e^{i\omega t}\,dx \tag{10}$$

factoring out α and rewriting equation (10) gives

$$F_\alpha = -\rho U^2 l^2 \alpha \int_0^1 \left\{\left[\frac{\partial S(x)}{\partial x}(1 - ik_1\sigma) + \frac{\partial S(x)}{\partial x}ik_1 x + 2S(x)ik_1 - k_1^2 S(x)(x - \sigma)\right]\right\} e^{i\omega t}\,dx \tag{11}$$

However,

$$\int_0^1 \frac{\partial S(x)}{\partial x}dx = 0$$

for a body pointed at both ends, therefore

$$F_\alpha = -\rho U^2 l^2 \alpha \int_0^1 \left[ik_1 x\frac{\partial S(x)}{\partial x} + iS(x)2k_1 + k_1^2 S(x)(\sigma - x)\right] e^{i\omega t}\,dx \tag{12}$$

The corresponding moment due to rotation is

$$M_\alpha = l\int_0^1 \frac{\partial F_\alpha}{\partial x}(x - \sigma)\,dx \tag{13}$$

Applying equation (9) to equation (13) gives

$$M_\alpha = -\rho U^2 l^3 \alpha \int_0^1 (x - \sigma)\left[\frac{\partial S(x)}{\partial x}(1 - ik_1\sigma) + \frac{\partial S(x)}{\partial x} ik_1 x + 2ik_1 S(x) + k_1^2 S(x)(\sigma - x)\right] e^{i\omega t}\, dx \tag{14}$$

Simplifying equation (14) and noting

$$\int_0^1 \frac{\partial S(x)}{\partial x}\, dx = 0$$

gives

$$M_\alpha = -\rho U^2 l^3 \alpha \int_0^1 \left[x \frac{\partial S(x)}{\partial x}(1 - ik_1\sigma) + ik_1(x^2 - x\sigma)\frac{\partial S(x)}{\partial x} + 2ik_1(x - \sigma)S(x) - k_1^2 S(x)(\sigma - x)^2\right] e^{i\omega t}\, dx \tag{15}$$

The force due to translation is

$$F_h = -\rho U^2 l^2 \int_0^1 \left(\frac{\partial}{\partial x} + ik_1\right) S(x) \frac{w(x)}{U} e^{i\omega t}\, dx \tag{16}$$

where

$$w(x) = \dot{h} = i\omega h_o = i \frac{\omega l}{U} U \frac{h_o}{l} = ik_1 U \frac{h_o}{l}$$

Simplifying equation (16) and substituting for $w(x)$ gives

$$F_h = -\rho U^2 l^2 \frac{h_o}{l} \int_0^1 \left[\frac{\partial S(x)}{\partial x} \frac{ik_1 U}{U} + ik_1 \frac{ik_1 U}{U} S(x)\right] e^{i\omega t}\, dx \tag{17}$$

noting that

$$\int_0^1 \frac{\partial S(x)}{\partial x} = 0$$

gives

$$F_h = +\rho U^2 l^2 k_1^2 \frac{h_o}{l} \int_0^1 S(x) e^{i\omega t}\, dx \tag{18}$$

The corresponding moment due to translation is

$$M_h = -l \int_0^1 (x - \sigma) \frac{\partial F_h}{\partial x} \, dx \tag{19}$$

Substituting equation (16) in equation (19) gives

$$M_h = -\rho U^2 l^3 \int_0^1 (x - \sigma)\left(\frac{\partial}{\partial x} + ik_1\right) S(x) \frac{w(x)}{U} e^{i\omega t} \, dx \tag{20}$$

Substituting $w(x) = ik_1 U \frac{h_o}{l}$ and simplifying equation (20) gives

$$M_h = -\rho U^2 l^3 \frac{h_o}{l} \int_0^1 (x - \sigma)\left[ik_1 \frac{\partial S(x)}{\partial x} - k^2 S(x)\right] e^{i\omega t} \, dx \tag{21}$$

noting that $\int_0^1 \frac{\partial S(x)}{\partial x} dx = 0$ makes equation (21) become

$$M_h = -\rho U^2 l^3 \frac{h_o}{l} \int_0^1 \left[ik_1 x \frac{\partial S(x)}{\partial x} - (x - \sigma) k_1^2 S(x)\right] e^{i\omega t} \, dx \tag{22}$$

Evaluation of the integrals found in the forces and moments was accomplished by numerical integration and were determined as follows:

$$\int_0^1 S(x) \, dx = \pi(0.1038)(0.05) = 0.01626 \tag{23}$$

$$\int_0^1 xS(x) \, dx = \pi(0.04298)(0.05) = 0.00674 \tag{24}$$

$$\int_0^1 x^2 S(x) \, dx = \pi(0.021370)(0.05) = 0.003355 \tag{25}$$

$$\int_0^1 x \frac{\partial S(x)}{\partial x} = 2\pi(-0.002107) = -0.01321 \tag{26}$$

$$\int_0^1 x^2 \frac{\partial S(x)}{\partial x} = 2\pi(-0.001948) = -0.01225 \tag{27}$$

Before substituting the moment in equation (1), assume simple harmonic motion, namely

$$\begin{aligned} h &= h_o e^{i\omega t} \\ \dot{h} &= h_o i\omega e^{i\omega t} \\ \ddot{h} &= -h_o \omega^2 e^{i\omega t} \\ \alpha &= \alpha_o e^{i\omega t} \\ \dot{\alpha} &= i\omega \alpha_o e^{i\omega t} \\ \ddot{\alpha} &= -\omega^2 \alpha_o e^{i\omega t} \end{aligned} \tag{28}$$

Every term in equations (1) and (2) will have an $e^{i\omega t}$ term so that $e^{i\omega t}$ may be divided out.

Substituting the values of the integrals in their appropriate places and then substituting the moment in equation (1) gives

$$\begin{aligned} &+\omega^2 I_\alpha \alpha_o + \omega^2 S_\alpha l \frac{h_o}{l} - C_\alpha \alpha_o + \left\{-\rho U^2 l^3 \frac{h_o}{l}\left[-ik_1(0.01321) - \right.\right. \\ &\left.(0.00674 - 0.01628\sigma)k_1^2\right] - \rho U^2 l^3 \alpha_o \left[-0.01321(1 - ik_1\sigma) - \right. \\ &ik_1(0.01225 - 0.01321\sigma) + 2ik_1(0.00674 - 0.01626\sigma) - \\ &\left.\left.k_1^2(0.01626\sigma^2 - 0.01348\sigma + 0.003355)\right]\right\} = 0 \end{aligned} \tag{29}$$

Grouping and combining terms gives

$$\begin{aligned} &\alpha_o \left\{+\omega^2 I_\alpha - C_\alpha - \rho U^2 l^3 \left[-0.01321 - k_1^2(0.01626\sigma^2 - 0.01348\sigma + 0.003355) + \right.\right. \\ &\left.ik_1(0.00123 - 0.00610\sigma)\right]\right\} - \frac{h_o}{l}\left\{-\omega^2 l S_\alpha + \rho U^2 l^3 \left[-ik_1(0.01321) - \right. \right. \\ &\left.\left.(0.00674 - 0.01628\sigma)k_1^2\right]\right\} = 0 \end{aligned} \tag{30}$$

Dividing equation (30) by $I_\alpha\omega^2$ and rearranging terms gives

$$a_o\left[+1-\left(\frac{\omega_\alpha}{\omega}\right)^2-\frac{\rho U^2 l^3}{I_\alpha\omega^2}\lambda_1\right]+\frac{h_o}{l}\left[+\frac{lS_\alpha}{I_\alpha}-\frac{\rho U^2 l^3\lambda_2}{I_\alpha\omega^2}\right]=0 \qquad (31)$$

where

$$\lambda_1 = -0.01321 - k_1^2(0.01626\sigma^2 - 0.01348\sigma + 0.003355) + ik_1(0.00123 - 0.00610\sigma)$$

and

$$\lambda_2 = -ik_1(0.01321) - k_1^2(0.00674 - 0.01628\sigma)$$

Making the substitutions of $k_1 = \frac{l\omega}{U}$

$$S_\alpha = \text{[illegible]}$$

$$I_\alpha = r^2M$$

$$\frac{I_\alpha}{\rho l^5} = K_1$$

make equation (31) into

$$\left[+1-\left(\frac{\omega_\alpha}{\omega}\right)^2-\frac{\lambda_1}{k_1^2K_1}\right]a_o+\left[+\frac{lz}{r^2}-\frac{\lambda_2}{k_1^2K_1}\right]\frac{h_o}{l}=0 \qquad (32)$$

Operating on equation (2) as was done on equation (1), namely, substituting the integrals and then the forces in equation (1) gives

$$+\omega^2S_\alpha a_o + M\omega^2h_o - C_hh_o + \rho U^2l^2k_1^2\frac{h_o}{l}\left[0.01626\right]+\left[-\rho U^2l^2a_o\right]\left[-ik_1(0.01321)+2ik_1(0.01626)+k_1^2(0.01626\sigma-0.00674)\right]=0 \qquad (33)$$

let

$$\lambda_3 = ik_1 0.0193 + k_1^2(0.01626\sigma - 0.0067\mu)$$

$$\lambda_\mu = 0.01626$$

and

$$K_2 = \frac{M}{\rho l^3}$$

Dividing equation (33) by $M\omega^2 l$, making the above substitutions, and rearranging terms gives

$$\left[\frac{z}{l} - \frac{\lambda_3}{k_1^2 K_2}\right] a_o + \left[1 - \left(\frac{\omega_\alpha}{\omega}\right)^2\left(\frac{\omega_h}{\omega_\alpha}\right)^2 + \frac{\lambda_\mu}{k_1^2 K_2}\right]\frac{h_o}{l} = 0 \qquad (34)$$

let $\Omega = \left(\frac{\omega_\alpha}{\omega}\right)^2(1 + ig)$ where g is the structural damping coefficient.[7]

The condition to have other than a trivial solution $\left(a_o = \frac{h_o}{l} = 0\right)$ of equations (32) and (34) is to have the determinant of the coefficients set equal to zero.

This determinant consists of

$$\begin{bmatrix} 1 - \Omega - \frac{\lambda_1}{k_1^2 K_1} & \frac{lz}{r^2} - \frac{\lambda_2}{k_1^2 K_1} \\ \frac{z}{l} - \frac{\lambda_3}{k_1^2 K_2} & 1 - \left(\frac{\omega_h}{\omega_\alpha}\right)^2 \Omega + \frac{\lambda_\mu}{k_1^2 K_2} \end{bmatrix} = 0 \qquad (35)$$

---

[7] Ben Smilg, and Lee S. Wasserman, "Application of Three-Dimensional Flutter Theory to Aircraft Structures." Air Corps Technical Report No. 4796, July, 1942.

It can be shown that this determinant has no solution for physical values of the frequencies. This is perhaps due to an oversimplification in the derivation of the forces and moments.

Flutter of the vented tube. Work on the forces due to internal flow through a vented tube has been discussed by Barton.[8] The acceleration forces on a particle of air are discussed by Seeley and Ensign.[9] The aerodynamic forces used in this analysis will be determined from the kinematics of the internal flow and from considerations of the potential flow over the cylinder. In the derivation of these forces the contributions due to rotational and translational motions are treated separately.

Considering the case of rotational motion, treat first the forces and moments arising from the deflection of the air stream through the tube, that is, the internal flow. The force is assumed to act at the front of the body and is given by

$$P_\alpha = -\pi\rho R^2 U^2 \alpha \tag{36}$$

The associated moment about the axis of rotation is

$$M_\alpha = \pi\rho R^2 U^2 \alpha S_1 \qquad \text{where } S_1 = \alpha l \tag{37}$$

The forces arising from the rotational velocity and accelerations are next considered.

---

[8] J. V. Barton, "The Effect of the Variation of Mass on the Dynamic Stability of Jet-Propelled Missiles." Journal of Aeronautical Sciences, Vol. 17, No. 11, November, 1950.

[9] Fred B. Seeley, and Newton E. Ensign, Analytical Mechanics for Engineers, Published by John Wiley and Sons, Inc., Chapter XIV, pp. 390-395.

The accelerations experienced by a particle moving along a path as the path rotates are (a) the accelerations the particle would experience if the path were fixed and the particle moved along the path, (b) the acceleration the particle would experience if it were fixed on the path and the path were permitted to move, and (c) the Coriolis component or the compound supplementary acceleration. Assuming that the streamlines are deflected through the angle α and are not curved relative to the axis of the tube, the resulting forces experienced by the particle are illustrated in Figure 14. The accelerations due to (a) are zero since there is no venturi and no burning inside the vented tube.

Integrating the differential force and differential moments about the axis of rotation over the volume of the tube yields the forces and moments exerted by the air on the tube. These integrals are

$$P_\alpha = -\rho \int_0^l \int_{-R}^{R} \int_{-\sqrt{R^2-y^2}}^{\sqrt{R^2-y^2}} \left\{2U\dot{\alpha} + \ddot{\alpha}(x - S_1)\right\} dz\, dy\, dx$$

$$M_\alpha = -\rho \int_0^l \int_{-R}^{R} \int_{-\sqrt{R^2-y^2}}^{\sqrt{R^2-y^2}} \left\{2U\dot{\alpha}(x - S_1) + \left[(x - S_1)^2 \ddot{\alpha}\right]\right\} dz\, dy\, dx \tag{38}$$

and reduce to

$$P_\alpha = -\rho\pi R^2 \ddot{\alpha}\left(\frac{l^2}{2} - S_1 l\right) - 2\rho\pi R^2 U\dot{\alpha} l$$

$$M_\alpha = -\rho\pi R^2 \ddot{\alpha}\left(-S_1{}^2 l + S_1 l^2 - \frac{l^3}{3} - \frac{R^2 l}{4}\right) - \rho\pi R^2 U\dot{\alpha} l(l - 2S_1) \tag{39}$$

The differential forces and moments due to the external flow about the tube due to rotational motion may be approximated by considering the tube infinite in length and evaluating equation (6) for the appropriate

downwash distribution. Integration of the differential force and moment yields

$$P = -\pi\rho R^2 \left(\frac{l^2}{2} - S_1 l\right) \ddot{\alpha}$$
$$M = -\pi\rho R^2 \left(\frac{-l^3}{3} + S_1 l^2 - S_1 l\right) \ddot{\alpha} \tag{40}$$

The total forces and moments due to rotation are

$$P = -\pi\rho R^2 \left[\left(\frac{l^2}{2} - S_1 l\right) \ddot{\alpha} + U^2 \alpha\right] - \pi\rho R^2 \ddot{\alpha} \left(\frac{l^2}{2} - S_1 l\right) - 2\pi\rho R^2 U \dot{\alpha} l$$
$$M = -\pi\rho R^2 \left[\left(-\frac{l^3}{3} + S_1 l^2 - S_1 l\right) \ddot{\alpha} - U^2 S_1 \alpha\right] - \pi\rho R^2 \ddot{\alpha} \left(-S_1^2 l + S_1 l^2 - \frac{l^3}{3} - \frac{R^2 l}{4}\right) - \pi\rho R^2 U \dot{\alpha} (l - 2S_1) \tag{41}$$

For the case of translation a treatment similar to that given for rotation is employed.

The internal flow yields, as a result of momentum changes, the following forces and moments

$$P = -\pi\rho R^2 U \dot{h}$$
$$M_\alpha = \pi\rho R^2 U S_1 \dot{h} \tag{42}$$

The forces and moments arising from accelerations (refer to Figure 14) integrate to

$$P = -\pi\rho R^2 l \ddot{h}$$
$$M_\alpha = -\pi\rho R^2 \left(\frac{l^2}{2} - S_1 l\right) \ddot{h} \tag{43}$$

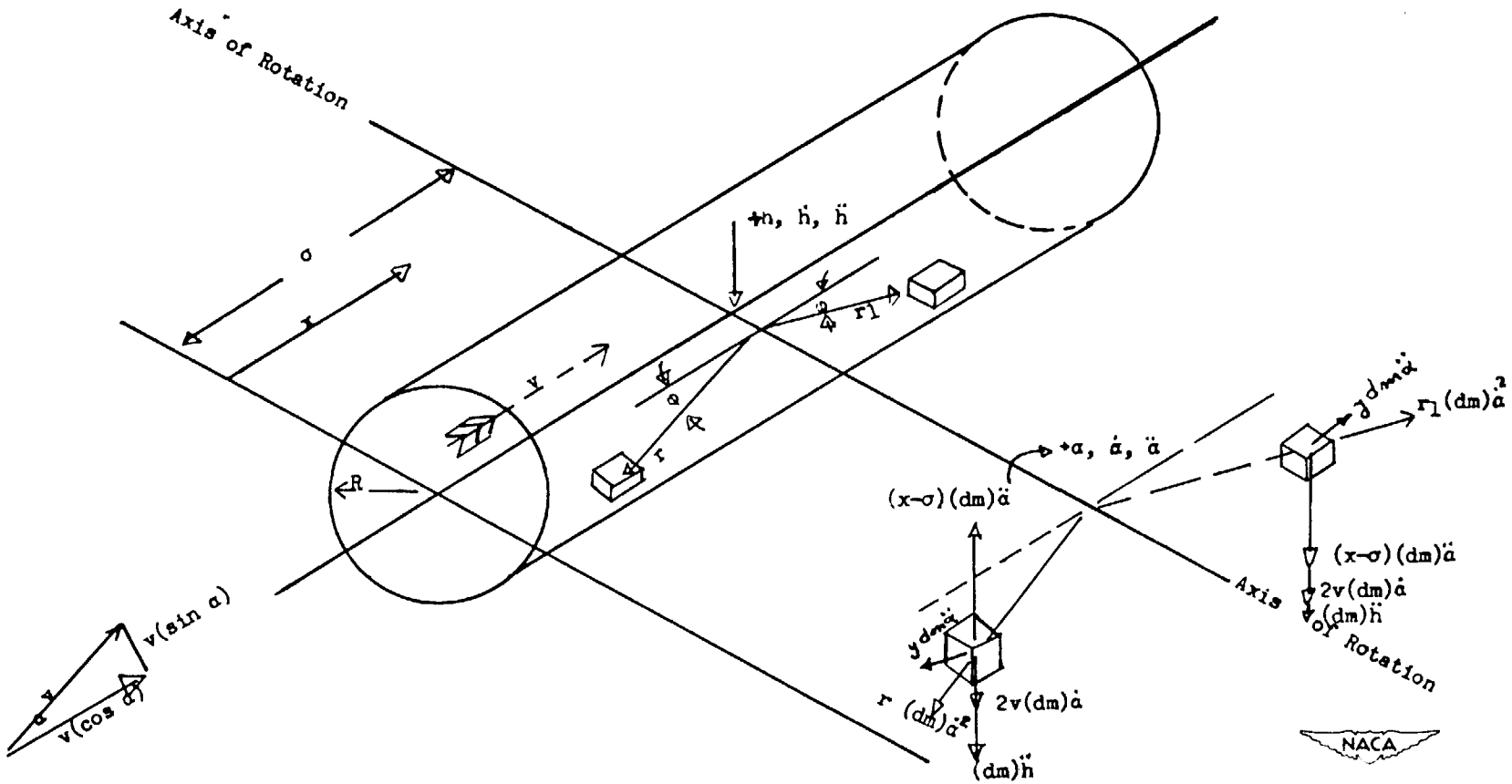

Figure 14.- Forces acting on elements of fluid due to $\dot{\alpha}$, $\ddot{\alpha}$, and $\ddot{h}$ for open tube.

The external flow yields the following

$$P = -\pi\rho R^2 l\ddot{h}$$

$$M_a = -\pi\rho R^2 \left(\frac{l^2}{2} - S_1 l\right)\ddot{h} \tag{44}$$

The total forces and moments due to translation are

$$P = -\pi\rho R^2(U\dot{h} + 2l\ddot{h}) - \pi\rho R^2 U\dot{h}$$

$$M = -\pi\rho R^2 \left\{\left(\frac{l^2}{2} - S_1 l\right)2\ddot{h} + \left(\frac{l}{2} - S_1\right)U\dot{h}\right\} +$$

$$\pi\rho R^2 U\dot{h}S_1 \tag{45}$$

Summing the forces and moments due to rotation:

	Force	Moment
Change of momentum arising from consideration of the force acting at the front of the tube	$-\pi\rho R^2 U^2\alpha$	$\pi\rho R^2 U^2\alpha S_1$
Coriolis component	$-2\pi\rho R^2 U l\dot{\alpha}$	$\pi\rho R^2 lU\alpha(2S_1 - l)$
Acceleration the particle would have if the path were fixed and the particle free to move	0	0
Acceleration the particle would have if it were fixed on the path and the path were free to move	$\pi\rho R^2\ddot{\alpha}\left(S_1 l - \frac{l^2}{2}\right)$	$-\pi\rho R^2\ddot{\alpha}\left(-S_1^2 l + S_1 l^2 - \frac{l^3}{3} - \frac{R^2 l}{4}\right)$
External force and moment assuming tube to be infinite in length	$\pi\rho R^2\ddot{\alpha}\left(S_1 l - \frac{l^2}{2}\right)$	$-\pi\rho R^2\ddot{\alpha}\left(S_1^2 l - S_1 l^2 + \frac{l^3}{3}\right)$

Summing the forces and moments due to translation:

	Force	Moment
Change in momentum	$-\pi\rho R^2 U\dot{h}$	$\pi\rho R^2 l U\dot{h}$
Translatory acceleration of the air particles	$-\pi\rho R^2 \ddot{h} l$	$\pi\rho R^2 \ddot{h}\left(S_1 l - \frac{l^2}{2}\right)$
External force	$-\pi\rho R^2 \ddot{h} l$	$\pi\rho R^2 \ddot{h}\left(S_1 l - \frac{l^2}{2}\right)$

Again assume harmonic motion and substitute the total moment and force in equations (1) and (2), respectively. After making the substitutions that

$$\Omega = \left(\frac{\omega_h}{\omega}\right)^2 (1 + ig)$$

$$k = \frac{b\omega}{v_f}$$

$$S_\alpha = Mz$$

$$C_\alpha = I_\alpha \omega_\alpha^2$$

$$I_\alpha = Mr^2$$

$$\lambda_1 = \frac{l^2}{2} - lS_1$$

$$\lambda_2 = 2l\left(\frac{l^2}{3} - lS_1 + S_1^2 + \frac{R^2}{8}\right)$$

$$\phi_1 = \frac{M}{\pi\rho R^2}$$

$$\phi_2 = \frac{\pi\rho R^2}{I_\alpha}$$

and regrouping terms, equation (1) becomes

$$\frac{h_o}{l}\left[-\frac{zl}{r^2}-\phi_2(ibS_1 l+2\lambda_1 l)\right]+a_o\left[-1+\left(\frac{\omega_a}{\omega_h}\right)^2\Omega-\phi_2\left(\frac{b^2S_1}{k^2}+\lambda_2-\frac{2ib\lambda_1}{k}\right)\right]=0$$

and equation (2) becomes

$$\frac{h_o}{l}\left[-l-l\Omega+\frac{l}{\phi_1}\left(\frac{ib}{k}-2l\right)\right]+a_o\left[-z+\frac{1}{\phi_1}\left(\frac{b^2}{k^2}+\frac{2ibl}{k}-2\lambda_1\right)\right]=0$$

The condition to have other than a trivial solution $\left(a_o=\frac{h_o}{l}=0\right)$ of the above two equations is to set the determinant of the coefficients equal to zero. This determinant is as follows:

$$\begin{bmatrix} -\frac{z}{r^2}-\phi_2\left(\frac{ibS_1}{k}+2\lambda_1\right) & -1+\left(\frac{\omega_a}{\omega_h}\right)^2\Omega-\phi_2\left(\frac{b^2S_1}{k^2}+\lambda_2-\frac{2ib\lambda_1}{k}\right) \\ -1-\Omega+\frac{l}{\phi_1}\left(\frac{ib}{k}-2l\right) & -z+\frac{1}{\phi_1}\left(\frac{b^2}{k^2}+\frac{2ibl}{k}-2\lambda_1\right) \end{bmatrix}=0$$

A sample solution will be shown. The parameters used correspond to the first line of data in Table III, page 21. The evaluation of the parameters in the determinant is as follows:

$z = 0.10$ $\qquad$ $\phi_2 = 0.00482$

$r^2 = I_a/M = 0.6203$ $\qquad$ $l = 2.5$

$I_a = 0.0875$ $\qquad$ $\lambda_2 = 2.643$

$M = 0.1410$

$\phi_1 = 335.0$

$b = 1.25$

$S_1 = 1.25$

$\lambda_1 = 0.0$

$\frac{\omega_a}{\omega_h} = 8.40/3.10 = 2.71$

The determinant becomes

$$\begin{bmatrix} -0.16122 - \frac{0.007528i}{k} & 7.3424\Omega - \frac{0.0094i}{k^2} - 1.0127 \\ \Omega + \frac{0.003731i}{k} - 1.0149 & -0.10 + \frac{0.04664}{k^2} + \frac{0.01865}{k^2} \end{bmatrix} = 0$$

For an assumed value of $1/k$ of 4,

$$\Omega_1 = 0.1574 - 0.001769i = \left(\frac{\omega_h}{\omega}\right)^2(1 + ig)$$

Ω_2 indicates a negative frequency and is of no interest. Thus,

$$\left(\frac{\omega_h}{\omega}\right)^2 = 0.1574$$

and

$$g = \frac{0.001769}{0.1574} = 0.0112$$

A series of $1/k$'s are assumed until a curve connecting the values intersects with the $g = 0.03$ line as shown on Figure 15.

This value of $1/k$ is operated on to obtain $\frac{v_f}{b\omega_a}$ as follows:

$$\frac{\left(\frac{1}{k}\right)\left(\frac{\omega_h}{\omega_a}\right)}{\frac{\omega_h}{\omega}} = \frac{v_f}{b\omega_a}$$

or

$$\frac{8.28}{0.484}\,\frac{1}{2.71} = 6.35$$

The flutter frequency ratio $\frac{\omega_h}{\omega}$ is plotted against $1/k$ so that the corresponding frequency ratio may be chosen. This ratio $\frac{\omega_h}{\omega}$ is divided into the structural frequency ratio $\frac{\omega_h}{\omega_a}$ to obtain $\frac{\omega_f}{\omega_a}$ or $\frac{f_f}{f_a}$.

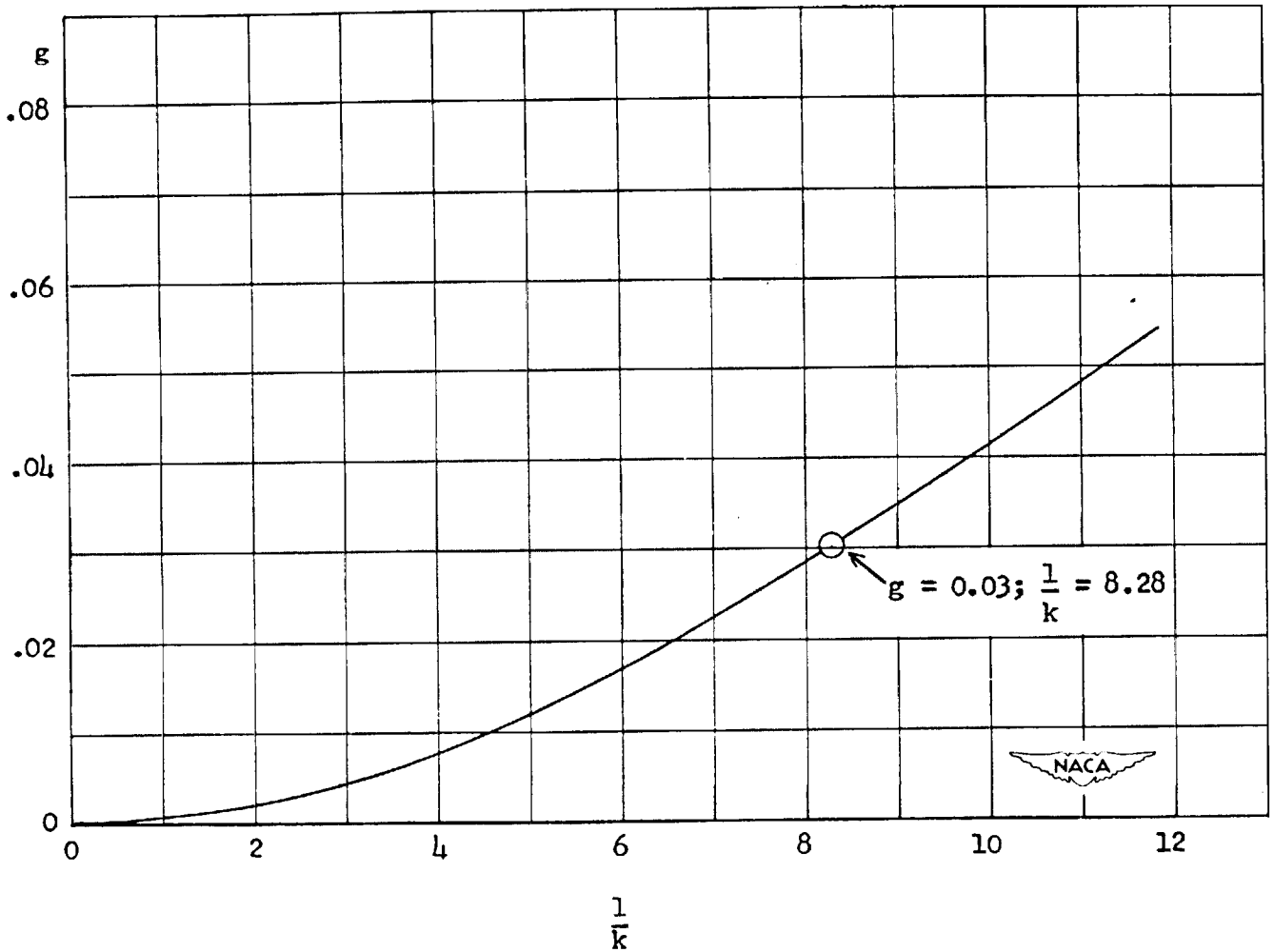

Figure 15.- Variation of theoretical structural damping coefficient g with reduced frequency parameter 1/k for the vented tube configuration.

The results of these flutter calculations have been tabulated on Tables II and III (pages 20 and 21) and are plotted on Figures 16 and 17.

DIVERGENCE

As previously defined, divergence occurs when the aerodynamic moment is greater than the restoring moment. Therefore by equating the aerodynamic moment to the restoring moment, an equilibrium velocity can be determined. Any velocity greater than the determined velocity will result in divergence of the system. The restoring moment for the supporting struts for both configurations is $k_\alpha(\alpha)$ where k_α is the torsional spring constant in foot pounds per radian and α is the angle of attack in radians. The aerodynamic moment is not obtained as easily.

Allen of NACA in a paper entitled "Estimation of the Forces and Moments Acting on Inclined Bodies of Revolution of High Fineness Ratio," added a term to include viscosity to the aerodynamic moment determined by Munk.

Munk's moment is

$$\frac{1}{q}\frac{dM}{d\alpha} = -2(K_2 - K_1)\ \text{Vol.}$$

or

$$M_\alpha = -2(K_2 - K_1)\ \text{Vol.}\ q\alpha$$

Allen's modified moment equation is

$$M_\alpha = -2\left[\text{Vol.} - S_b(l - x_m)\right]\ q\alpha + \eta C_{d_c} A_p (x_m - x_p) q\alpha^2$$

where the terms are defined as follows:

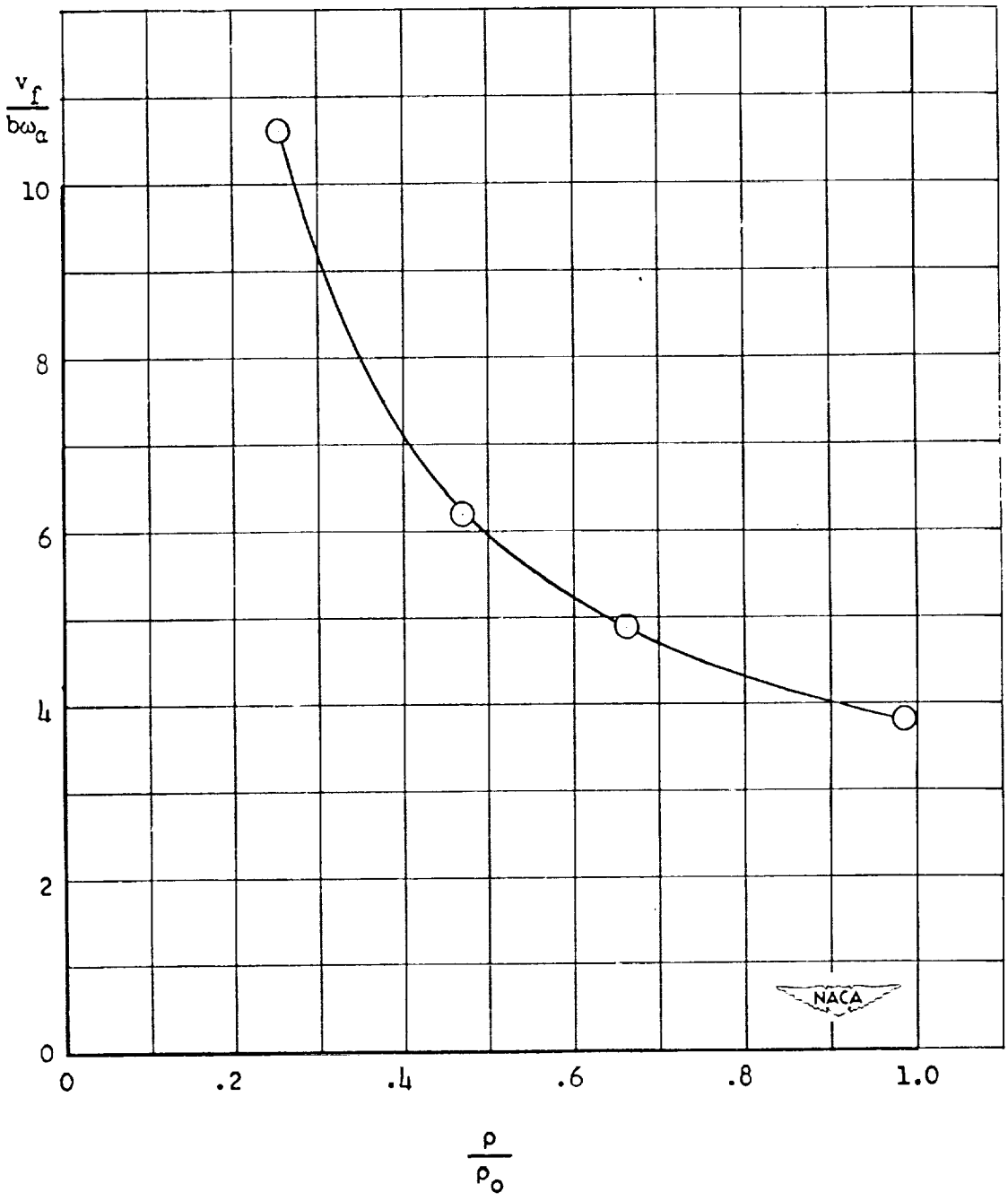

Figure 16.- Variation of theoretical flutter speed coefficient with density coefficient for the open-tube configuration.

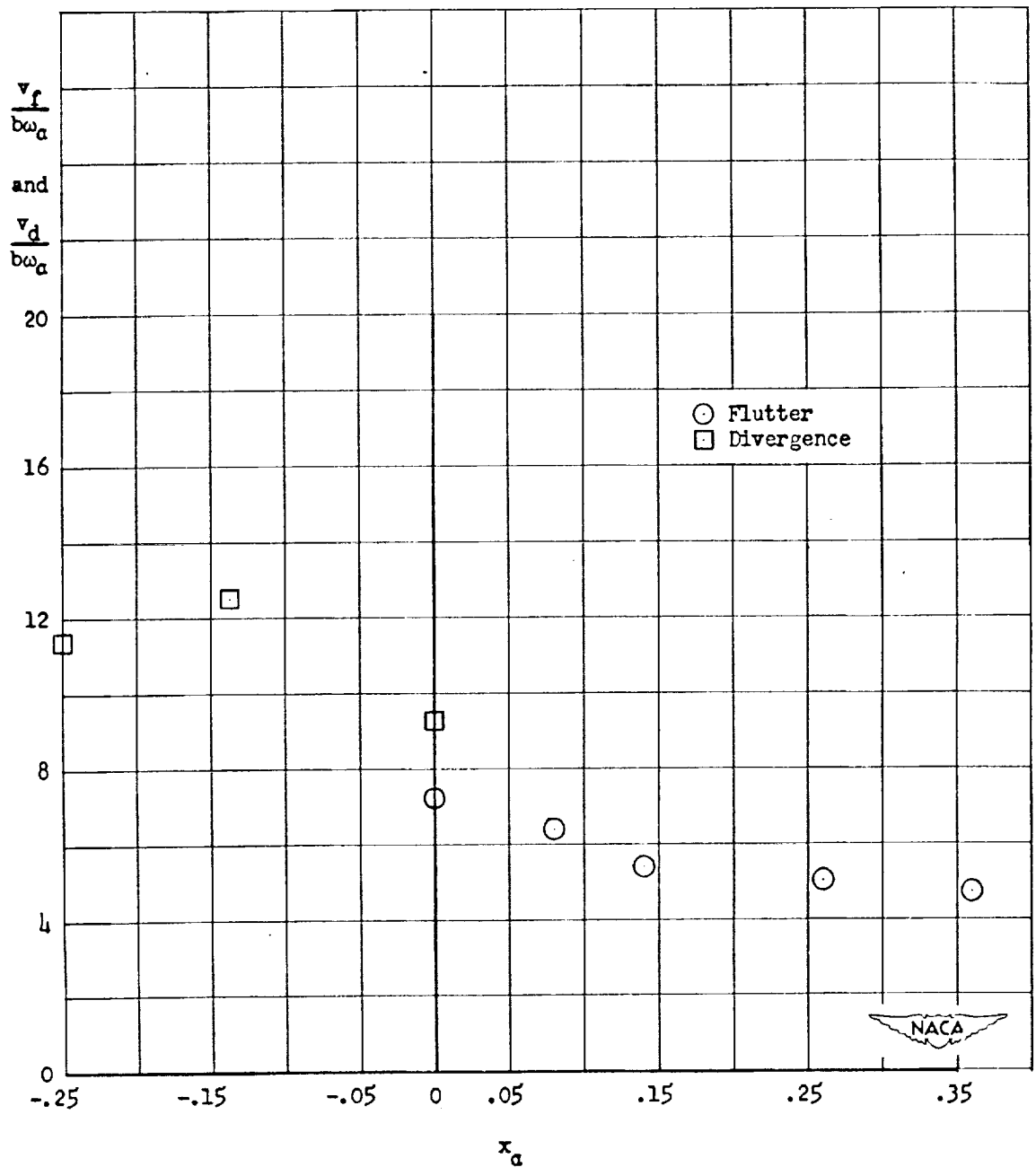

Figure 17.- Variation of theoretical flutter speed and divergence speed coefficients with nondimensional center-of-gravity position x_α for the open-tube configuration.

M_α moment in foot pounds

$(K_2 - K_1)$ Munk's longitudinal and transverse apparent mass coefficient, for Allen's equation; $(K_2 - K_1) = 1$

Vol. volume of body of revolution, cubic feet

S_b cross-sectional area of the base of the body, square feet

l body length, feet

x_m station of axis of moments, feet

q dynamic pressure, pounds per square foot $\frac{1}{2} \rho v_d^2$

α angle of attack, radians

η drag coefficient ratio, function of length to diameter ratio of body of revolution

C_{d_c} section drag coefficient, function of Mach and Reynolds numbers

A_p plan-form area, square feet

x_p distance of the centroid of the plan-form area from the bow, feet

Supplying values to Allen's equation based on the 65020 airfoil-shaped body, the following constants are obtained

Vol. = 0.249 cubic feet

$S_b = 0$

$l = 2.5$ feet

$x_m = 0$

$\eta = 0.62$

$C_{d_c} = 1.20$

$A_p = 0.64ct = 0.64 \times 0.5 \times 2.5 = 0.80$

$x_p = 1.25$

$\rho = 0.002378$

The equation now reads

$$M_\alpha = -2(0.249 - 0)\tfrac{1}{2} \times 0.002378 v^2 \alpha + 0.62 \times 1.2 \times 0.80(0 - 1.25)\frac{0.002378}{2} v^2 \alpha^2$$

$$M_\alpha = -0.000592 v^2 \alpha - 0.000885 v^2 \alpha^2$$

Setting the aerodynamic moment equal to the restoring moment:

$$0.000592 v^2 \alpha + 0.000885 v^2 \alpha^2 = k_\alpha \alpha$$

$$v^2 = \frac{k_\alpha}{0.000592 + 0.000885\alpha}$$

$$v = \sqrt{\frac{k_\alpha}{0.000592 + 0.000885\alpha}}$$

k_α = 2695 inch pounds per radian corresponding to the data of Table I

$$k_\alpha = \frac{2695}{12} = 247 \text{ foot pounds per radian}$$

therefore

$$v = \sqrt{\frac{247}{0.000592 + 0.000885\alpha}}$$

From the above expression it is seen that the divergence speed is affected by angle of attack. Assume α very small for these tests, therefore

$$v = \sqrt{\frac{247}{0.000592}} = \sqrt{41.9 \times 10^4}$$

v = 644 feet per second. Another calculation of the divergence speed for the airfoil-shaped body based on the derived oscillating moment will be given.

The oscillating aerodynamic moment for the airfoil-shaped body is given as equation (15) on page 41. Since for torsional divergence k is zero, this equation reduces to

$$M_\alpha = -\rho v^2 l^3 a(-0.01321) \tag{46}$$

The restoring moment is defined as

$$k_t \alpha = I_\alpha \omega_\alpha{}^2 \alpha \tag{47}$$

Equating equations (46) and (47) and solving for v gives

$$v_d = \sqrt{\frac{I_\alpha \omega_\alpha{}^2}{\rho l^3 (0.01321)}}$$

since $l = 2.5$

$$v_d = 2.21 \omega_\alpha \sqrt{\frac{I_\alpha}{\rho}}$$

The divergence speed corresponding to the first data point of Table I (page 19) is

$$v_d = 2.21(2.82)(2\pi)\sqrt{\frac{0.06900}{0.00054}} = 441 \text{ ft/sec}$$

The divergence speed corresponding to the data of Table V (pages 29 and 30) is

$$v_d = 2.21(9.25)(2\pi)\sqrt{\frac{0.00670}{0.00232}} = 690 \text{ feet/sec}$$

The aerodynamic moment for the open tube configuration is given as equation (41) on page 48. For the case of divergence, ω is zero and the equation reduces to

$$M_\alpha = \pi \rho R^2 v^2 S_1 \alpha$$

Equating this moment to the restoring moment and solving for v gives

$$v_d = \omega_\alpha \sqrt{\frac{I_\alpha}{\pi \rho R^2 S_1}}$$

where

$$S_1 = 1.25$$

$$R = 0.25$$

therefore

$$v_d = 2.02 \omega_\alpha \sqrt{\frac{I_\alpha}{\rho}}$$

The divergence speed corresponding to the first line of the data of Table II (page 20) is

$$v_d = 2.02(2.40)(2\pi)\sqrt{\frac{0.08640}{0.00055}} = 380 \text{ ft/sec}$$

The divergence speed corresponding to the first line of the data of Table III (page 21) is

$$v_d = 2.02(8.4)(2\pi)\sqrt{\frac{0.08750}{0.00214}} = 671 \text{ ft/sec}$$

The divergence speed coefficients $\frac{v_d}{b\omega_\alpha}$ have been calculated and are found on Table III, page 21.

TORSIONAL INSTABILITY

For single-degree-of-freedom torsional flutter for the airfoil-shaped body, the differential equation of motion is

$$-I_\alpha \ddot{\alpha} - C_\alpha \alpha + M_\alpha = 0 \qquad (48)$$

where M_α is given in equation (15) on page 41. For harmonic motion equation (48) becomes

$$I_\alpha\omega^2\alpha_o - C_\alpha\alpha_o - \rho v^2 l^3 \alpha_o \left[-0.01321 - 4k^2(0.01626\sigma - 0.01348\sigma + 0.003355) + 2ik(0.00123 - 0.00610\sigma)\right] = 0 \qquad (49)$$

The imaginary part of the equation must be zero so that

$$2k(0.00123 - 0.00610\sigma) = 0$$

or values $k = 0$, $\sigma = 0.2015$ give solutions.

The $k = 0$ gives the divergence condition while $\sigma = 0.2015$ allows flutter solutions. However, should structural damping be included other values of k and σ will allow solutions.

The real part of the equation becomes

$$I_\alpha\omega^2 - C_\alpha - \rho v^2 l^3 \left[-0.01321 - \frac{\omega^2 l^2}{v^2}\lambda\right] = 0 \qquad (50)$$

where

$$\lambda = (0.01626\sigma^2 - 0.01348\sigma + 0.003355) = +0.001300$$

$$\omega^2 - \omega_\alpha{}^2 + \frac{\rho v^2 l^3}{I_\alpha}(0.01321) + \frac{\rho\omega^2 l^5}{I_\alpha}\lambda = 0 \qquad (51)$$

or

$$\omega = \sqrt{\frac{\omega_\alpha{}^2 - 0.01321\,\frac{\rho v^2 l^3}{I_\alpha}}{1 + \frac{\rho l^5}{I_\alpha}\lambda}} \qquad (52)$$

From equation (52) it may be seen that for a specific test condition the instability frequency decreases with increasing velocity. An illustration of the order of magnitude of the results may be obtained by

inserting values from Table IV (page 27) in equation (52). A sample calculation will be made using the first test data on this table.

$$\omega = \sqrt{\frac{(2\pi 10.1)^2 - 0.01321\ \frac{(0.0023)(299)^2\ (2.5)^3}{0.0670}}{1 + \frac{(0.0023)(2.5)^5\ (0.00130)}{0.0670}}}$$

$\omega = 57.4$ or $f_t = 9.14$ cps.

The curve of the change in instability frequency with airspeed is shown in Figure 18, and the values are given in Table IV, page 27.

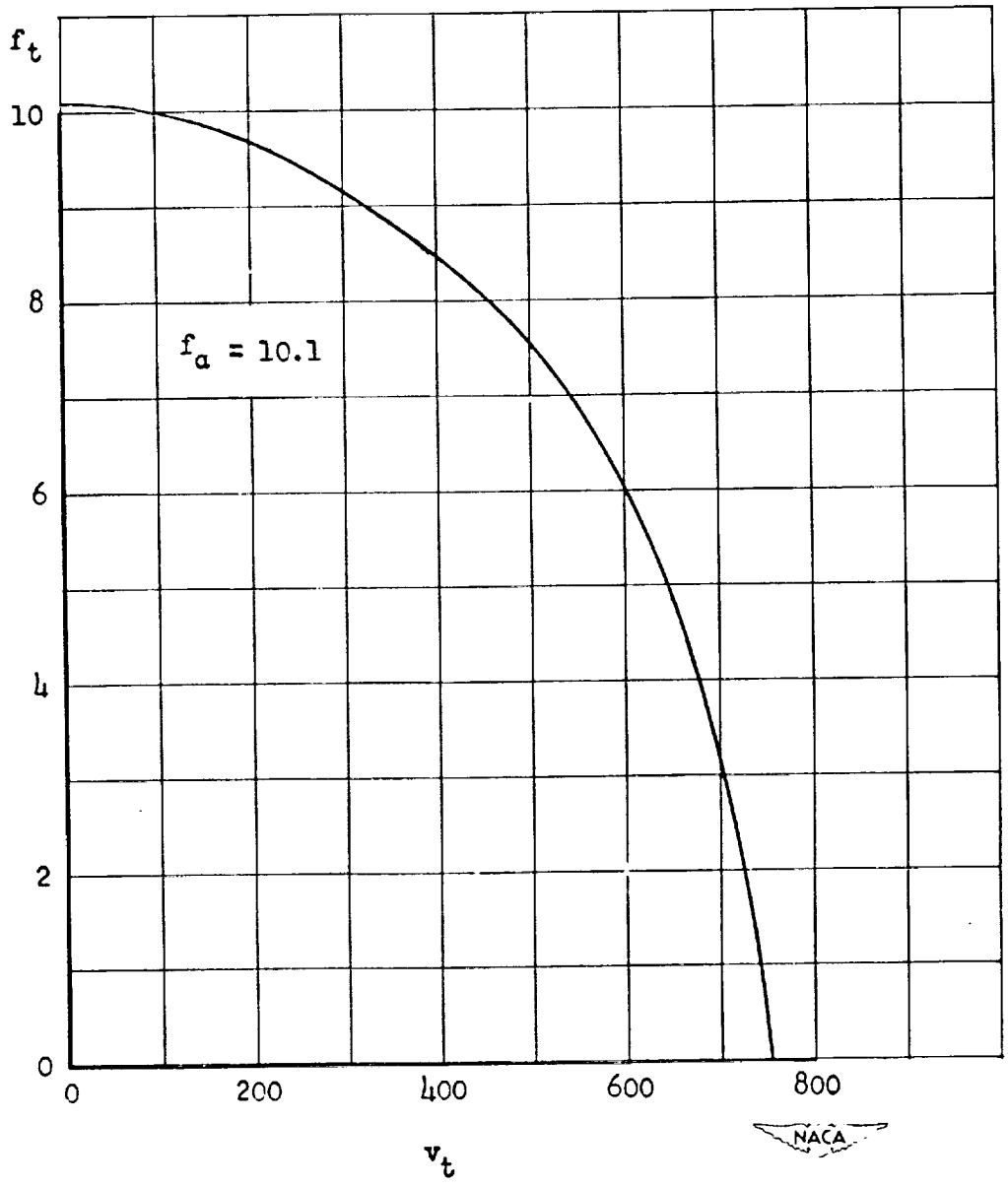

Figure 18.- Variation of the theoretical instability frequency with airspeed for the airfoil-shaped body.

CHAPTER VI

COMPARISON OF ANALYSES WITH EXPERIMENT

This chapter presents a comparison of the results of the analyses with the experimental data on flutter, divergence, and torsional instability.

FLUTTER

There was no comparison made between experimental data and the flutter analysis for the airfoil-shaped body since the analysis yielded no results.

The comparisons of analyses with experimental flutter data for the vented tube configuration showed very good agreement. The calculations showed both the trend (Table II, page 20) and magnitude (Table III, page 21) of the flutter speed coefficients. The calculations showed the trend of the flutter frequency parameters, whereas the calculated flutter frequencies were higher than the experimental flutter frequencies.

DIVERGENCE

Since no divergence data was obtained and no experimental speeds were attained as high as the analysis predicted for divergence, no comparison can be made between experimental data and analysis for the airfoil-shaped body.

Comparison of the experimental divergence speed with the analytical divergence speed for the open tube showed little agreement. For the same configuration ($a = 0$) $v_{d_{Exp.}}$ was approximately 400 fps and $v_{d_{Ana.}}$ was 671 fps. The ratio of speeds is 0.596.

TORSIONAL INSTABILITY

From the analysis for single-degree-of-freedom torsional flutter, it was found that for one position of center-of-gravity location ($\sigma = 0.2015$ or c.g. at 20 per cent chord) and assuming zero structural damping, flutter would occur. The torsional flutter frequency would decrease with increasing airspeed. Experimentally, the frequency did decrease with increasing airspeed. A comparison of Figure 18 with Figure 10 showed that the analytical instability frequency decreased approximately as the experimental instability frequency.

CHAPTER VII

SUMMARY AND CONCLUSION

Summary. Results of experimental tests of flutter and divergence of large masses at ends of short struts are presented. Two basic configurations were tested; (1) an open tube having provision for various nose and rear sections, and (2) a body of revolution based on the NACA 65020 airfoil section. Flutter was obtained on both basic configurations. There was no experimental divergence data to compare with analysis for the airfoil-shaped body configuration. A single-degree-of-freedom torsional instability was experienced when certain nose and rear sections were installed on the open tube. A similar instability was encountered on the airfoil-shaped body when the stiffer struts were used. Some of the effects of density and center-of-gravity position on flutter of the vented tube were observed.

Analytical investigations are presented for flutter, divergence, and torsional instability. These analyses showed little agreement with experimental data.

Conclusions. Conclusions for this experimental and analytical investigation may be enumerated as follows:

1. Flutter speed coefficients increased with decrease in density for both basic configurations.

2. Flutter frequency remained essentially constant for changing density for both configurations.

3. Flutter speed coefficient is essentially independent of center-of-gravity position for the open tube when the c.g. was varied as in these tests.

4. Flutter occurred when the c.g. was behind the elastic axis and divergence occurred when the c.g. was ahead of the elastic axis.

5. Torsional instability was encountered with the tube for certain nose and rear section installations.

6. The effect of density on the instability speed coefficient of the tube with hemisphere nose and rear sections was similar to that on the flutter speed coefficient, namely, that as the density decreased, the instability speed coefficient increased.

7. The instability frequency of the above-mentioned configuration remained constant with changing density.

8. Analytical flutter speeds showed good agreement with experiment both as to trend and magnitudes for the vented tube configuration.

9. The analysis for the airfoil shaped body of revolution yielded no results.

10. The calculated divergence speeds and frequencies showed good agreement with experimental data.

11. The calculated torsional instability frequencies showed good agreement with experimental torsional instability frequencies.

BIBLIOGRAPHY

1. Abbott, Ira H., "Airship Model Tests in the Variable Wind Tunnel." NACA Rep. 394.

2. Freeman, Hugh B., "Force Measurements on a 1/40 Scale Model of the Airship Akron." NACA Rep. 432.

3. Hoerner, S., "The Aerodynamics of Three Dimensional Bodies." McDonnell Aircraft Corp., Rep. No. GT-37.

4. Jones, Robert T., and Margolis, K. M., "Flow over a Slender Body of Revolution." NACA TN 1081.

5. Krgywoblocki, M. Zbigniew, "Investigation of the Wing Wake Frequency with Application of the Strouhal Number." Journal of Aeronautical Sciences, January, 1945, Vol. 12, No. 1.

6. Lin, C. C., Reissner, E., and Tsien, H. S., "On Two-Dimensional Non-Steady Motion of a Slender Body in a Compressible Fluid." Journal of Mathematics and Physics, No. 27, pp. 220-231, 1949.

7. Miles, J. W., "On Non-Steady Motion of Slender Bodies." Aeronautical Quarterly, Vol. II, Pt. 3, November, 1950, pp. 183-194.

8. Munk, Max M., "The Aerodynamic Forces on Airship Hulls." NACA Rep. No. 184.

9. Runyan, Harry L., and Sewall, John L., "Experimental Investigation of the Effects of Concentrated Weights on the Flutter Characteristics of a Straight Cantilever Wing." NACA TN 1594.

10. Seeley, Fred B., and Ensign, Newton E., Analytical Mechanics for Engineers, John Wiley and Sons, Inc., Third Edition, 450 pp.

11. Smilg, Benjamin, and Wasserman, Lee S., "Application of Three-Dimensional Flutter Theory to Aircraft Structures." Air Corps Technical Report 4798, July, 1942.

12. Smilg, Benjamin, "The Instability of Pitching Oscillations of an Airfoil in Subsonic Incompressible Flow." Journal of Aeronautical Sciences, Nov., 1949, Vol. 16.

13. Theordorsen, T., "General Theory of Aerodynamic Instability and the Mechanism of Flutter." NACA Rep. 496.

14. Theordorsen, T., and Garrick, I. E., "Mechanism of Flutter--A Theoretical and Experimental Investigation of the Flutter Problem." NACA Rep. 685.